Chapter 4

Hygroscopicity Measurements of Atmospherically Relevant Organic Aerosol Species[*]

---

[*] This chapter is prepared for journal submission as “Hygroscopicity Measurements of Atmospherically Relevant Organic Aerosol Species” by V. Varutbangkul, T. A. Rissman, F. J. Brechtel, D. O. Topping, G. B. McFiggans, R. C. Flagan, and J. H. Seinfeld.

4.1 Abstract

Hygroscopic growth of various organic aerosols in the subsaturated regime is investigated using the humidified tandem differential mobility analyzer (HTDMA). The compounds studied include dicarboxylic acids (oxalic, malonic, succinic, glutaric, adipic, and phthalic acids), amino acids (DL-leucine and DL-glutamic acid monohydrate), multifunctional acids (DL-malic, cis-pinonic, 2-hydroxycaproic, and sinapic acids), fatty acids (myristic, palmitic, and stearic acids), and cholesterol. Particles are generated by atomizing a solution of the organic compound in methanol in order to minimize water retained on the particle at low RH. Such retained water has been suggested as a possible reason for recent observations of laboratory-generated aerosols exhibiting smooth water uptake curve without any deliquescence behavior even when they are thought to be dry. Our results show that succinic acid, adipic acid, cholesterol, and the large fatty acids do not exhibit any water uptake at high RH even when allotted over 90 s of growth time in the mixing chamber. Cis-pinonic acid, 2-hydroxycaproic acid, phthalic acid, and sinapic acid show modest growth throughout the RH range studied. The growth curve obtained for DL-malic acid compares well with literature data and with predictions from the Aerosol Diameter Dependent Equilibrium Model (ADDEM) of Topping et al. (2005b), while results from malonic acid and glutaric acid are subject to an artifact that may be related to methanol retained in the aerosol phase or an unaccountable amount of suppression of particle evaporation at higher RHs. Oxalic acid growth factors fall within the variability of past studies. Observations of change in particle size with RH also suggests that dry particles of certain species, such as oxalic acid, DL-leucine, and DL-glutamic acid monohydrate particles may contain void volumes that collapse with

increasing RH, although the water uptake at higher RHs overcomes the reduction in particle size for oxalic and glutamic acids. A curve with a three-parameter empirical form is fitted through the experimental data for each organic species that exhibits water uptake. In general, despite using methanol atomizing solution, we do not observe deliquescence behavior in any species investigated, and surprisingly, the hygroscopic growth curves constructed from our data are consistent with wet particles observed in other studies. The possible explanations for this observation are discussed. Results from this study show continuous water uptake at a broad range of RHs and represent the first study in which laboratory-generated, atmospherically relevant organic aerosols have been generated in the absence of liquid water and at extremely low RH.

4.2 Introduction

Many properties of atmospheric aerosol depend strongly on the particle size and phase: atmospheric lifetime, optical properties, ability to serve as CCN, chemical reactivity, and even respiratory tract deposition characteristics. The hygroscopicity of a particle plays an important role in determining the particle size and phase at a given relative humidity (RH) and is thus one of the key fundamental properties that influence the magnitude of these aerosol impacts. For instance, the scattered light intensity due to aerosols, which is a key module in the calculations of the earth's radiation budget, varies as the particle diameter to the sixth power.

The hygroscopicity of a particle is related to the particle composition, and ambient aerosols are a complex mixture of inorganic as well as organic species. While the water uptake properties of many atmospherically relevant inorganic compounds are well known, the hygroscopicity of the organic fraction, which can comprise hundreds of species, remains poorly understood. Field studies have shown that 20–70% of particulate-phase organic carbon is water soluble (Saxena and Hildemann, 1996). This water-soluble fraction consists of a large variety of species such as dicarboxylic acids, multifunctional acids, alcohols, carbonyl compounds, nitrates, and amino acids. Numerous past studies have studied the water uptake behavior of these compounds in the laboratory using various experimental methods on both pure and mixed systems (Hansson et al., 1990; Cziczo et al., 1997; Cruz and Pandis, 2000; Peng et al., 2001; Peng and Chan, 2001; Prenni et al., 2001; Brooks et al., 2002; Choi and Chan, 2002a, 2002b; Hameri et al., 2002; Brooks et al., 2003; Chan and Chan, 2003; Prenni et al., 2003; Wise et al., 2003; Brooks et al., 2004; Gysel et al., 2004; Mikhailov et al., 2004; Parsons et al., 2004; Chan et al., 2005). These studies reveal that organic compounds exhibit a complex growth behavior that can depend strongly on the state of the aerosol sampled. The organic particles often exhibit a smooth water uptake with respect to relative humidity, sometimes starting at relatively low RHs, accompanied with very low efflorescence RH and/or very high deliquescence RH. In addition, the organics have been found to alter the water uptake of a coexisting inorganic phase in unexpected ways (Saxena et al., 1995). In fact, a recent study reports that even a monolayer of a hygroscopic organic species on an otherwise hydrophobic core can induce restructuring of the particle and markedly increase the scattering and absorption coefficients of the core particle at high RH (Mikhailov et al., 2006).

Although particles in the atmosphere are unlikely to exist as pure single-component organic particles, the hygroscopic growth data of a pure organic species are valuable because they can be used for first-order prediction of the hygroscopic growth in mixed systems (Cruz and Pandis, 2000; Choi and Chan, 2002b; Prenni et al., 2003; Wise et al., 2003). In addition, such data often provides input parameters for improving thermodynamic models that are used to predict hygroscopic or even the CCN activation behaviors (Peng et al., 2001; Topping et al., 2005a, 2005b).

Previous measurements of water uptake by pure organic particles suggested that the smooth hygroscopic growth curve and lack of deliquescence behavior at higher RH could indicate that the “dry” particles detected at the reference state (usually ~5% RH) are actually concentrated solutions (Peng et al., 2001; Prenni et al., 2001; Chan et al., 2005). The residual water could affect the water uptake behavior of the particle as well as assist particle activation in the supersaturated regime, affecting measurements of CCN activation (Huff Hartz et al., 2006). In this study, we investigate the hygroscopic growth in the subsaturated regime of pure organic particles generated by atomization from a methanol solution. In the companion study, methanol is used as the solvent to generate particles for CCN activation investigation as well. The type of water-free particles used in this study could be representative of secondary organic aerosol (SOA) formed in the atmosphere by gas-to-particle conversion or of other organic species condensing onto a non-deliquesced substrate, in which liquid water is absent due to the humidity history of the particle.

4.3 Experimental methods

4.3.1 Aerosol generation

Aerosol particles are generated by atomizing a solution of the organic compound of interest in methanol using a stainless steel, constant-flow atomizer. High-purity methanol is chosen as the solvent in order to minimize the amount of residual water in the atomized aerosol, which is usually generated from an aqueous solution. Methanol vapor is scrubbed out of the air surrounding the particles exiting the atomizer using a four-stage drying scheme, consisting of one silica gel diffusion dryer (50 cm in length, 3 cm in inner diameter), two 5-Å type molecular sieves diffusion dryers (90 cm each in length, 3 cm in inner diameter), and a Nafion dryer (model PD-200T-12SS, Perma Pure LLC, Toms River, NJ). While the Nafion dryer is marketed for water removal applications, its membrane, a copolymer of perfluoro-3,6-dioxa-4-methyl-7-octene-sulfonic acid and Teflon (polytetrafluoro-ethylene), also reportedly removes over 90% of methanol from the sample air (http://www.permapure.com/OurTechnology.htm). The purge air to this

Nafion dryer is room air that is dried through two packed silica gel cartridges, so as to not introduce any extra water vapor to the already dry sample stream.

The need for such an extensive drying system is due to the fact that the methanol solution is atomized extremely quickly due to the low surface tension compared to water—typically about 50 mL of solution is consumed every hour. This, coupled with the fact that methanol is very volatile, leads to the need for as complete removal of methanol in the vapor phase as possible. While small amounts of methanol left over in the gas stream may not significantly influence the water uptake of the aerosol being studied, it was found that an artifact would be introduced in the measurement due to the fact that our humidity probes (operating on the principle of capacitance) are also sensitive to volatile polar solvents such as methanol. Therefore, left-over methanol is detected as a false elevated relative humidity. For example, if only the silica gel diffusion dryer and one molecular sieves diffusion dryer are used to dry the aerosol stream, the "RH" detected of the resulting sample would rise slowly to 25–30% in 10 hours, due to the adsorbent being spent given the copious amount of methanol. This is unacceptable, as we would not be able to distinguish what portion of the RH signal is due to methanol and what portion is due to actual water vapor (the relative response of the probe to methanol is not characterized). If a Nafion dryer is added to the above system, the RH elevation is reduced to ~15%. Adding an additional molecular sieve diffusion dryer to this system results in an RH elevation of only ~1% after 10 hours. This allows accurate measurement of RH throughout the entire experiment, and the RH of the air exiting the drying system is maintained at 1–3%. The silica gel and molecular sieves in all diffusion and packed dryers are regenerated under heat and vacuum before each experiment.

The suite of compounds studied in this work is shown in Table 4.1. These include six dicarboxylic acids including simple straight-chain diacids from C_2 to C_6 (oxalic acid, malonic acid, succinic acid, glutaric acid, and adipic acid) in addition to phthalic acid (an aromatic diacid), two amino acids (DL-glutamic acid monohydrate and DL-leucine), four other multifunctional carboxylic acids (DL-malic acid, cis-pinonic acid, 2-hydroxycaproic acid, and sinapic acid), and finally three fatty acids (myristic acid, palmitic acid, and stearic acid) and cholesterol—a steroid. All experiments are performed at room temperature ($T = 25.5 \pm 0.8$ °C). The atmospheric relevance of these classes of compounds is discussed in the results and discussion section.

4.3.2 Hygroscopicity tandem differential mobility analyzer (HTDMA)

The HTDMA (Liu et al., 1978; Rader and McMurry, 1986; McMurry and Stolzenburg, 1989) is a widely used method to measure changes in submicron particle size with RH. The instrument used here is based on that described previously (Varutbangkul et al., 2006), but with slight modifications in the CPC unit and humidification system. A schematic of the setup is illustrated in Fig. 4.1. The dried aerosol sample is first passed through a TSI ^{85}Kr charger (Model 3077, TSI Inc., St. Paul, MN) to achieve equilibrium charge distribution and is then classified at constant voltage in the first cylindrical DMA (Model 3071, TSI Inc, St. Paul, MN) to a specified diameter, usually 60 and/or 180 nm, depending on the size distribution of the aerosol generated by the atomizer. Larger classified sizes are sometimes used for compounds prone to significant evaporation. A hygrometer probe (Model HMP233, Vaisala Inc., Woburn, MA) is used to monitor the RH of the sheath flow in the first DMA.

Changing the RH of the carrier air is achieved by passing the filtered excess flow from the classifying DMA through a custom 18-tube Nafion membrane moisture exchanger (Model PD-070-18T-12SS, Perma Pure LLC, Toms River, NJ). The Nafion humidifier, while technically called a “dryer” by the manufacturer, can be used to humidify air flow if a humid air stream is supplied on the purge side at a flow rate of approximately twice the flow rate of the flow to be humidified. Dry air from a silica gel scrubber and water-saturated air from a heated water bubbler are mixed together at a controlled ratio to make up this Nafion purge air, the moisture from which is transferred to the excess flow of the classifying DMA. The humidification system can be bypassed, allowing verification of the classified aerosol size.

Monodisperse aerosol from the classifying DMA is mixed with the RH-conditioned air in an insulated, laminar flow mixing column, which has a residence time of approximately 38 s. The particles undergo hygroscopic growth in this column and enter the second DMA, operating in scanning mode to measure the new aerosol size distribution. The scanning DMA sheath flow is also drawn from the humidification column; in this manner, the organic vapor is preserved, and re-partitioning of the organics between the particle and gas phase, which may alter the aerosol water affinity and content, is reduced. Two hygrometer probes (Model HMM211, Vaisala Inc., Woburn, MA) are used to measure the temperature and RH immediately before and after the scanning DMA on the sheath and excess flows. Classified particles from the scanning DMA are detected with a TSI Model 3010 CPC with dilution flow from filtered room air. Both DMAs are operated at 2.5 L/min sheath and excess flow rates and 0.25 L/min aerosol and monodisperse flow rates. The particle size classification by the DMAs has been validated by sampling polystyrene latex (PSL) spheres of known sizes (Duke Scientific Corp., Palo Alto, CA).

Inversion of the scanning DMA data (Collins et al., 2002) yields the size distribution of the grown droplets, which can then be fitted with a lognormal curve to obtain a mode diameter corresponding to the peak of the distribution. The hygroscopic growth factor (*GF*) at a certain RH is then defined as the ratio of the diameter of the humidified particle, $D_{p,wet}$, to that of the dry classified particle, $D_{p,dry}$:

$$GF = \frac{D_{p,wet}}{D_{p,dry}} \tag{4.1}$$

Due to particle evaporation in the mixing column between the first and second DMA, the dry particle size $D_{p,dry}$ is not necessarily equal to 60 or 180 nm as expected from the first DMA. The reference diameter for growth factor determination is the particle size that is measured when the humidification system is bypassed and the classified aerosol is allowed to pass through the mixing column in dry air. When the humidification system is bypassed, the temperature and the particle residence time are unaffected as only the particle-free air stream (excess flow of classifying DMA) is rerouted.

The RH in the HTDMA is varied from 0–3% (no humidification) up to 90% in order to measure the dependence on growth factor on RH. The humidity probes are regularly calibrated against a set of saturated salt solutions in the range of 11%–93% RH, and the RH readings are corrected according to the linear fit from such a calibration. The HTDMA measurement is validated with ammonium sulfate, the growth factor of which as a function of RH is well known (Tang and Munkelwitz, 1994; Nenes et al., 1998). The HTDMA is found to be able to reproduce the hygroscopic growth curve that agrees to within 0.02 in *GF* compared to theoretically calculated *GF* of 1.484 at 80% RH (Nenes et al., 1998), equivalent to an error of about 1.5% (n=18). The precision of the measurement, measured from the same $(NH_4)_2SO_4$ experiment, is 1% (n=18). However, additional uncertainties are introduced in the organic experiments performed in this work, relating to the dependence of the dry reference diameter after classification on particle evaporation and retained solvent, as will be discussed in the forthcoming section. Therefore, we report a conservative uncertainty of ±0.04 in *GF* for this study.

To investigate the effect of particle size on growth factor, the HTDMA is set to switch between classifying 60-nm and 180-nm particles (unless otherwise noted) after three complete up- and down-scan cycles at each size. There is a 70-s delay between the switch in the classifying DMA high voltage and the start of the second DMA's scanning at the new size to prevent contamination. For certain compounds, due to the atomization process and the nature of the organic species, there is a limitation in the particle sizes that can be classified that yield good counting statistics for the scanning DMA, in which case, either only one size of 60 or 180 nm is selected, or a different diameter is chosen.

Chan and Chan (2005) recently reported that an issue in a number of hygroscopic growth studies is insufficient time to attain equilibrium particle size. Thus, we adopt an optional mode of operation utilizing another mixing column in series with the existing one, which allows the particles more time to grow. The additional column is a stainless steel tube 4.7 cm in diameter and 140 cm long, thus allowing an additional 53 seconds in residence time for the particles to reach equilibrium, after the 38 seconds in the first mixing column. This "two-column" mode of operation is sometimes used to verify that the measured growth factors reflect particles at equilibrium, assuming that the kinetics of the mass transfer is fast enough that the additional 53 seconds afforded by the second column will result in additional growth if residence time was an issue.

A full hygroscopic growth curve is constructed by plotting the growth factor values versus the relative humidity. To fit a curve through such experimental data, we employ a general equation of the following empirical functional form:

$$GF = 1 + \left[\left(1 - \frac{RH}{100} \right)^{-A} * B \left(\frac{RH}{100} \right)^{C} \right] \tag{4.2}$$

where RH is the relative humidity expressed between 0 and 100, and A, B, and C are positive empirical parameters. Varutbangkul et al. (2006) found that this functional form, which combines two existing fit equations, is more useful than either of the two forms alone in representing hygroscopic growth data of SOA generated from oxidation of cycloalkenes and biogenic terpenes. While some species studied in this work can be satisfactorily fit with a more traditionally used power-law fit represented by the right-hand multiplicative term (Wise et al., 2003), other species exhibit growth curves that are more appropriately fit with Eq. 4.2 above, similar to in the SOA system. We will thus report the fit parameters in the context of the above equation and set A to 0 when the data is better fit with a pure power-law form alone. Finally, our hygroscopic growth curves are compared with available literature data as well as model predictions of water uptake according to the ADDEM model as described below.

4.3.3 ADDEM thermodynamic model

The details of the Aerosol Diameter Dependent Equilibrium Model (ADDEM) and its use in the sub-saturated humid regime have been described previously both for inorganic systems (Topping et al., 2005a) and for organic and mixed organic/inorganic systems (Topping et al., 2005b). In short, the model combines a direct minimization of the Gibbs free energy within an iterative loop which solves the original Köhler equation. In this manner, diameter-dependent calculations of *GF* can be made. For calculating the activity coefficients of organic solute in solution, the widely used group-contribution method UNIFAC (Fredenslund et al., 1975), supplemented by modified functional group interaction parameters according to electrodynamic balance data of low-molecular weight diacids (Peng et al., 2001), is employed. The pairs of interactions with modified parameters include COOH-H_2O, OH-H_2O, and OH-COOH pairs, which are most affected by hydrogen bonding and thus previously led to a limitation in the use of UNIFAC for species with strongly polar groups separated by less than 3–4 carbons (Fredenslund and Sorensen, 1994). With the original UNIFAC equations and these revised interaction parameters, Peng et al. (2001) and Topping et al. (2005b) found that the predictions for atmospherically relevant species were improved considerably. The model was shown to adequately describe mixed systems including 5–6 dicarboxylic acids, down to low relative humidity conditions.

Although the Kelvin term in the Koehler theory, which takes into account the effect of particle curvature on the water activity, is not expected to play a very large role in the calculation of equilibrium RH at our particle sizes, the Kelvin effect can still be considered explicitly in this scheme using a variety of surface tension models. The first ("S1") utilizes the Tamura mixing rule (Tamura et al., 1955). The second ("S2") uses the Suarez thermodynamic method (Suarez et al., 1989), the assumption of constant molar surface area, and calculated activity coefficients according to UNIFAC as discussed above. The third and probably most accurate surface tension model ("S3"), uses the Li and Lu thermodynamic model, in which the saturated surface excess and adsorption constant parameters are fit to the recent experimental data by Gyula Kiss and Stefano Decesari (unpublished data). The activity coefficients are again calculated using UNIFAC with the revised interaction parameters of Peng et al. (2001). These three types of surface tension inputs to the models yield *GF* values that are within 1.1% of each other at up to 90% RH with the particle diameters in this study. This is well within the experimental uncertainty. Thus, only the results of "S3" will be presented in comparison with our growth curves. Due to limited availability of surface tension model input parameters as well as difficulty in using the fundamental Kohler theory for systems which exhibit phase separation, model predictions are currently only available for the straight-chain dicarboxylic acids and malic acid.

Topping et al. (2005a) found that there are large sensitivities of *GF* calculations on the value of dry density used. Therefore, the nature of the drying process, which can influence the final crystalline form of aerosols generated for HTDMA studies, may be important in introducing systematic uncertainties upon comparisons with such theoretical predictions. We will thus discuss our findings in light of these sensitivities of the model.

4.4 Results and discussion

4.4.1 Dicarboxylic acids

Dicarboxylic acids are emitted both through primary anthropogenic emissions and through secondary organic aerosol formation by oxidation of gas-phase biogenic and anthropogenic hydrocarbons. Diacids have commonly been identified in the water-soluble organic fraction in atmospheric aerosol and cloud and rain water (Kawamura et al., 1996; Sempere and Kawamura, 1996; Kerminen et al., 2000; Rohrl and Lammel, 2001). Oxalic acid (C_2) is generally the most abundant diacid, followed by malonic acid (C_3) and succinic acid (C_4). In this study, we investigate the hygroscopic growth of six straight-chain diacids from C_2 to C_6, as well as an aromatic diacid: phthalic acid. As indicated in Table 4.1, previous studies (both experimental and theoretical) have shown an odd-even alternation in vapor pressures of the straight-chain diacids, with respect to their carbon number (Bilde et al., 2003). This parity-dependent phenomenon applies to the water solubility of the compound as well, which has implications on the hygroscopicity of the diacid particle. This could in turn influence the atmospheric lifetime of these species, as more hygroscopic particles would tend to be more CCN-active and thus removed more readily as precipitation. Removal of less hygroscopic particles may instead depend more on scavenging and coagulation.

Succinic acid and adipic acid

As shown in Figure 4.2, our study shows that the larger even-carbon-number diacids—succinic (C_4) and adipic (C_6) acids—do not take up water even at higher RHs, indicated by the growth factor of unity for both 60-nm and 180-nm classified particles at all RHs studied. This lack of hygroscopic growth is consistent with the high deliquescence relative humidity (DRH), which is the RH at which dry, solid particles absorbs water and become a solution, of both compounds, determined by various experimental and modeling studies. The DRH of succinic acid at room temperature is estimated to be in the range of 91–100% (Saxena and Hildemann, 1997; Peng et al., 2001; Prenni et al., 2001; Brooks et al., 2002; Ming and Russell, 2002; Wise et al., 2003; Parsons et al., 2004), while adipic acid DRH is estimated at 93–99% (Prenni et al., 2001; Brooks et al., 2002; Parsons et al., 2004). These high DRHs are outside the humidity range of this study; thus, the particles remain crystalline and do not exhibit any water uptake. This observation also agrees with previous studies, in which hygroscopic growth was not detect for initially dry succinic acid (Prenni et al., 2001; Wise et al., 2003) and adipic acid particles (Prenni et al., 2001; Hameri et al., 2002). Because the ADDEM thermodynamic model predicts the growth curve of the efflorescence branch (i.e., that of a deliquesced particle), our results do not lend themselves for comparison with the prediction.

Oxalic acid

In our oxalic acid (C_2) experiment, insufficient 180-nm particles could be classified from the atomized aerosol, regardless of the amount of solute added to the atomizer solution. Thus, only 60-nm particles are selected. Under dry conditions and after passing through our mixing column, these particles are detected by the second DMA with diameters between 41.5 and 43.8 nm. The shrinkage could be caused by two factors. First, the oxalic acid particle could evaporate/sublimate due to its sufficiently high vapor pressure and possible loss of organic vapor in the filters on the excess or sheath flow. Second, any methanol that may have been trapped inside the particle could evaporate if there are cracks or pores in the particles, leading to structural collapse of the particle. In any case, we proceed with using this reduced diameter as the dry diameter to calculate the growth factors for the moment.

The filled circles in Figure 4.3 show the *GF*s calculated from two oxalic acid experiments, each using a fresh atomizer solution. As indicated by *GF* values less than unity, we observe a considerable further reduction in particle size as compared to the dry size starting at 10% RH, with a minimum in "droplet" diameter at ~40% RH. This type of reduction in particle diameter with humidity has been observed in studies of wide-ranging chemical systems including carbon and diesel soot particles (Weingartner et al., 1997), freshly nucleated particles from CH_2I_2 ozonolysis in the presence of UV light (Jimenez et al., 2003), and internally mixed particles of the protein bovine serum albumin and NaCl (Mikhailov et al., 2004). In each of these works, the authors hypothesized that the dry particles are composed of porous agglomerates, either due to irregular or branched structures within the particle, or to ion-protein interactions/electric charge effects as proposed by Mikhailov et al. (2004). These agglomerate structures can then undergo compaction upon exposure to water vapor due to capillary condensation effects. The exact morphology and shape of our atomized and aggressively-dried particles is unknown, and the aerosol could potentially have void volumes that lead to structural rearrangement with increasing water vapor as well. Note that evaporation of the oxalic acid particle cannot account for the reduction in size observed at moderate RHs because the reference diameter already reflects the maximum evaporation of dry particles after a full residence time in the mixing chamber. It is unlikely that evaporation could be accelerated when particles are in solution.

In any case, we can attempt to recover the true growth curve from this bowl-shaped curve by assuming to first order that at the RH corresponding to the lowest point of the existing growth curve (in this case ~40% RH), the particle exists in its most compact form with negligible amount of bound water. We can then use the minimum diameter measured at this point as the new reference diameter to compute adjusted growth factors at higher humidities. Discarding the data points below the new reference RH, we obtain "adjusted" hygroscopic growth curves that are slightly shifted upward for the two experiments. These are indicated by the blue and green diamonds in Figure 4.3. Because the inherent assumption in this correction is that the particles contain negligible amount of water at the new reference RH (which may or may not be the case), the adjusted *GF*s represent a lower bound of the true *GF* values based on water-free particles.

Despite this complication, our adjusted data from two different experiments agree to within experimental uncertainty (±0.04 in *GF*). A curve in the form of Eq. 4.2 is fitted through the data from both experiments, and Table 4.2 lists these fit parameters as well as the *GF* value at 85% RH calculated from the fit. Also evident from Figure 4.3 is the significant scatter in the existing literature data for oxalic acid. In general, our results lie within the range of literature values and very close to the results of Koehler et al. (2006), who presented data originally published by Prenni et al. (2001) after correcting for particle evaporation. None of the experimental data seem to trend with model predictions, however, which are shown in the dashed and dash-dotted lines. This could be due to an error in parameter inputs to the model or an effect of the particle state and humidity history, as will be discussed below.

The DRH of oxalic acid is estimated to be 93–99% (Saxena and Hildemann, 1997; Peng et al., 2001; Prenni et al., 2001; Brooks et al., 2002; Wise et al., 2003). There is a considerable range of efflorescence relative humidity (ERH, also known as crystallization RH or CRH) reported in literature, ranging from 52 to 57% in an electrodynamic balance study by Peng et al. (2001) to <5% as observed in HTDMA and aerosol flow tube-FTIR studies by Braban et al. (2003) and Prenni et al. (2001), respectively. This discrepancy is likely due to the fact that supermicron particles levitated in the EDB experiments are millions of times greater in volume than those in HTDMA or flow tube experiments, and the probability of the formation of a critical embryo in the supersaturated liquid scales with the deliquesced particle volume, resulting in an issue of time scale due to crystallization kinetics. In this respect, it is not surprising that our results are consistent with other observations of submicron particles in that we do not observe any deliquescence behavior for oxalic acid particles. The adjusted hygroscopic curves are smooth, indicative of wet particles that have not effloresced, similar to the results of Prenni et al. (2001). It has been predicted that oxalic acid exists in its most stable form as anhydrous oxalic acid at <11% RH and as oxalic acid dihydrate at >11% RH (Baxter and Lansing, 1920). Braban et al. (2003) recently confirmed this aerosol phase transition at 12% ± 2% RH in their work using FTIR. Thus, the hygroscopic growth of oxalic acid could be modeled based on the dry density of either the anhydrous or the dihydrate form, and the dihydrate form exhibits a lower *GF* curve as shown in Figure 4.3. In both cases, the binary aqueous densities are calculated using the mass fraction mixing rule of Tang (1997) and Yen-Woods calculated organic liquid density of 1.478 g/cm^3 (Yen and Woods, http://www.pirika.com). However, our experimental data and literature values do not follow either of these curves.

The deviation of the model predictions from the measurements may be due to a number of reasons. First, Topping et al. (2005b) found that the model is sensitive to the dry density used in the calculation. When a lower dry density is used (dihydrate form, ρ

= 1.653 g/cm^3 (Weast and Astle, 1981)), the predicted growth curve is lower than that predicted using a higher dry density (anhydrous form, ρ = 1.9 g/cm^3 (Perry's Chemical Engineers' Handbook)). In this context, it is possible that the particles generated in the laboratory measurements, especially in HTDMA studies, which requires atomization from a liquid solution and subsequent drying, have an even smaller density due to porous morphology, regardless of whether the non-void fraction exists in the anhydrous or dihydrate form. The lowered density would be consistent with smaller *GF* measured. Adding to the sensitivity of the model to the assumed dry density is also the uncertainty in how the density of the solution varies with solute concentration, which is currently represented by the mixing rule according to Tang (1997).

The second possible reason for the disagreement between the model and the experimental *GF*s is that the interactions between ions in potentially very high-molality solutions could be poorly modeled even with the revised parameters of UNIFAC. In fact, according to Figure 2 in Peng et al. (2001), there seems to be only sufficient data for "improved" interaction parameters above an RH 60% for oxalic acid. Below this RH, the water cycle does not exhibit a smooth curve, making model extrapolations at lower RHs more uncertain. Fortunately, for other compounds, experimental data are available across wider ranges.

To explore the level of uncertainties in both issues raised above, Table 4.3 is used to illustrate that a significant range in oxalic acid *GF* predictions can be achieved depending on the combination of input parameters chosen for use in the model. These inputs include the UNIFAC parameter matrix values (Hansen et al. (1991) or Peng et al. (2001)), dry density value (anhydrous or dihydrate form), and liquid density value (solid anhydrous, solid dihydrate, water, or calculated organic liquid density from Yen-Woods method (Yen and Woods, http://www.pirika.com)). For a particle of 50 nm diameter at 90% RH, Table 4.3 shows that the S3 model can predict a *GF* in the range of 1.469–1.654, depending on which combination of input parameters is used. Thus, for oxalic acid, there is significant uncertainty in the model predictions as well. Such uncertainties are composition dependent, and oxalic acid appears to be unique among the systems in this study given both the uncertainty in the dry density and that due to the relatively small subset of conditions from which revised UNIFAC parameters are derived. In addition, the sensitivity to these uncertainties also appears to increase with decreasing particle size (Topping et al., 2005b).

To return to the discussion of the experimental results, however, it is interesting and somewhat surprising that our results are consistent with the results of Koehler et al. (2006) since our aerosols are generated from a high-purity methanol solution, which is water free. Care is also taken to dry any other diluting air stream that enters the system as much as possible. Thus, our particles are not expected to have been deliquesced at any point in the system, as they are never exposed to any RH above the RHD of at least 93%. Observations from Braban et al. (2003) demonstrate that it is indeed possible to dry out oxalic acid aerosols to efflorescence below 5% RH, as their dried particles exhibit no water uptake until the DRH. This raises the question of whether it is possible for the methanol solvent to form complexes with oxalic acid even at low RH and cause it to behave as if it is deliquesced with water. Even if this is the case, it appears that the absolute growth factor is not affected by the methanol-specific interactions, as our experimental data are close to those of Koehler et al. (2006).

On the other hand, the interpretation that our particles remain in solution even at low RH would be in conflict with our observation of reduced particle sizes at moderate RH, which instead suggests that the particle is porous and thus in the solid phase. One possibility that may bridge these two phenomena is that some methanol is trapped in the inner core of the particle, unable to escape to the vapor phase when the dry oxalic acid forms a “crust” over it, and this methanol acts to aid water uptake of the aerosol upon exposure to slight humidity, causing the particle to behave as if it were wet. The loss of this trapped methanol only at increased RH when the particle dissolves is then observed as a decrease in particle size (GF < 1) as long as the amount of water absorbed is less than the volume of methanol that is released. Given that the particle size is reduced by as much as 15% at maximum compaction, this would indicate a loss of 39% volume fraction of methanol that would need to be trapped inside the dry particle. This is a rather large amount of methanol, which seems somewhat unlikely. On the other hand, if the dry particle traps some methanol on the inside but contains some porous structure on the outside surface, the collapse of this outer structure could also account for some amount of size reduction as well (in addition to loss of methanol).

A remote possibility that would also bridge the two observations suggesting that the particles exhibit behaviors of both a solid and liquid particle is that the aerosol exists in an amorphous glass-like state in which a small amount of water or methanol is bound to the fractal surface. This bound solvent could cause a macroscopic behavior of a dissolved particle, while the particle could still contain void volume within the amorphous structure that allows compaction. Further studies could investigate the exact phase and morphology of the dry particles to determine the cause of these seemingly conflicting behaviors. Suffice it to say, given our observations, that the oxalic acid particles, once corrected for size reduction, exhibit a smooth water uptake as in the efflorescence branch similar to the data reported by Koehler et al. (2006). It is not yet possible to close model predictions with experimental results due to the uncertainties existing for both the theoretical frameworks and laboratory conditions.

Malonic acid and glutaric acid

Malonic acid (C_3) and glutaric acid (C_5) are odd-carbon-number diacids with larger vapor pressures than the neighboring diacids. They correspondingly exhibit very significant shrinkage due to evaporation after the first DMA. Therefore, much larger-size (400 nm) particles are selected for these two compounds to counteract the material loss. Figure 4.4a shows the size distribution of 400-nm classified glutaric acid particles detected in the scanning DMA after having flowed through the mixing chamber. The resulting distribution is bimodal, with a major peak at 225 nm and much smaller peak at 334 nm. When the dry particles are allowed to flow directly from the classifying DMA to the scanning DMA, bypassing the mixing chamber and reducing the residence time to only several seconds, there is less loss, and the size distribution is unimodal with a peak at about 323 nm, as shown in Figure 4.4b. This suggests that at the bottom of the mixing column where the dry particles are allowed to mix with humidified air, the size distribution is likely to be more similar to the larger-diameter mode seen in Figure 4.4a (at ~334 nm). Nevertheless, because both modes continue to appear in the grown droplet distribution at higher humidities (indicating that significant evaporation still occurs), we can calculate *GF* using both peaks. However, as shown in Figure 4.5, the resulting growth curves using either mode are anomalously high compared to existing literature data and the model prediction. This is also the case for malonic acid growth curve, which is shown in Figure 4.6a. The shape of these growth curves is also unusual and appears almost linear, with very little curvature compared to other species. The droplet sizes seem to increase very quickly with RH beginning at even very low RH.

When malonic acid aerosol is generated from an aqueous solution, however, a reasonable growth curve can be obtained after performing a correction for size reduction at moderate RH as is done in the case of oxalic acid. This result is illustrated in Figure 4.6b. Thus, the anomaly appears to be related to the particle generation using methanol solution, and could be due to retention of methanol in the particle even after drying. If the methanol forms complexes with the acids and does not evaporate away, it could cause much higher uptake of water simply due to methanol's affinity for water. This would also occur if the methanol was trapped inside the dry particle but is not released upon particle dissolution. Another possibility is that the presence of methanol in the particle somehow helps to suppress acid evaporation when a water film is also present, possibly by reducing the equilibrium vapor pressure of the acid further. If this methanol-induced suppression of evaporation is a function of the amount of liquid water (and thus the humidity), then the proper "dry diameter" from which *GF* is calculated is also a function of RH, and we would not be able to determine this proper reference diameter or calculate an accurate *GF*. In this case, the dry diameter we obtain by measuring the dry aerosol size distribution after the particles have traversed the mixing column will reflect maximum evaporation and thus minimum size. This would translate to anomalously high *GF* curves as observed in Figure 4.5 and 4.6a.

Note that the much larger percentage shrinkage in the methanol-atomized malonic acid particle (400 to 180 nm compared to 110 to 90 nm when atomized from aqueous solution) indicates that a large amount of methanol is retained even after thorough drying, and much of this retained solvent is released after the classification. It is possible that in future experiments, much longer time scales would be needed to allow for complete solvent evaporation from the particle after the drying process and before the particle classification.

As seen in Figure 4.6b, our malonic acid growth curve from an aqueous-solution experiment also shows no deliquescence behavior. This is most likely due to some retained water in the aerosol even at low RH after extensive drying, as also seen by Prenni et al. (2001). The DRH of malonic acid is estimated to be 65–91% at room temperature (Saxena and Hildemann, 1997; Peng et al., 2001; Brooks et al., 2002; Ming and Russell, 2002; Wise et al., 2003; Parsons et al., 2004). The ERH at room temperature has recently been measured at 18.6% (Parsons et al., 2004) using an optical microscope and flow cell for supermicron particles and 6% ± 3% (Braban et al., 2003) using FTIR and flow tube for submicron particles. If the latter measurement applies to our aerosol sizes, there is a possibility that our particles retain some water even though we measure RH of only 1–2% out of the atomizer even in the experiment with aqueous solution. Note that humidity measurement at such a low RH is also subject to increased uncertainty (± 3% according to the manufacturer's specifications). Also, with our post-evaporation particle size of 90 nm, ERH could be even lower than that observed by Braban et al. (2003) due to the previously mentioned effect of crystallization kinetics and particle volume dependence.

As for glutaric acid, the DRH is estimated to be 83–99% (Saxena and Hildemann, 1997; Cruz and Pandis, 2000; Peng et al., 2001; Brooks et al., 2002; Choi and Chan, 2002a; Ming and Russell, 2002; Wise et al., 2003; Parsons et al., 2004). The only known ERH measurement is by Peng et al. (2001) of 29–33%, but once again this is observed for a large supermicron particle and may not be applicable to the much smaller particles in this study. Prenni et al. (2001) were also unable to completely dry out glutaric acid particles, which exhibit smooth water uptake curve. The authors then placed a limit of <5% for the ERH of glutaric acid. Interestingly, Cruz and Pandis (2000) reported no water uptake by glutaric acid below 80% and a deliquescence transition at 85% RH, which suggests that they were able to generate effloresced particles. This variation serves as a reminder that particle history and nature of the drying process can greatly affect the particle phase and thus the water uptake behavior of the aerosol.

In any case, the methanol issue appears to override other effects to induce anomalous growth behaviors in our experiment. Water uptake measurement of glutaric acid particles generated from a water solution has not yet been performed but will likely yield similar results as in the malonic acid case—smooth growth curve that falls within the range of previous studies.

Phthalic acid

In addition to the straight-chain dicarboxylic acids discussed above, we also studied the hygroscopic growth of phthalic acid, which is an aromatic diacid that has been identified in ambient aerosol (Sempere and Kawamura, 1994, 1996; Ray and McDow, 2005) and is found to be structurally similar to metal binding sites in humic materials (Gamble et al., 1980). Hameri et al. (2002) studied the growth of internally mixed $(NH_4)_2SO_4$ and phthalic acid particles in an HTDMA and saw that they behaved similarly to internally mixed $(NH_4)_2SO_4$ and adipic acid particles. The authors then inferred that phthalic acid probably acted as a non-hygroscopic compound like adipic acid. However, Brooks et al. (2004) and Huff Hartz et al. (2006) studied phthalic acid in its pure form and found that it was slightly hygroscopic. Our results, shown in Figure 4.7, also confirm the hygroscopic nature of phthalic acid. Our 180-nm classified particles, which become 154 nm after evaporation, show growth factors that agree well with previous studies. The 60-nm classified particles, which shrink to 47 nm after evaporation, take up significantly more water. This could be explained by the fact that the smaller-sized particles are more prone to evaporation during the measurement of the dry classified size, and this evaporative loss is likely suppressed when the humidity is raised starting at the bottom of the mixing column. We could then be underestimating the initial dry particle diameter, which would lead to an erroneously high growth factor. This does not appear to be an issue for our 154-nm particles as the growth curve from those data points is consistent with literature data.

4.4.2 Amino acids

Water-soluble organic nitrogen compounds have been found to contribute about 18% of the total fine aerosol mass (Zhang et al., 2002). Of these nitrogen-containing compounds, amino compounds and free amino acids, possibly deriving from pollen or bacteria, have commonly been detected in ambient aerosols and fog droplets (Scheller, 2001; Zhang and Anastasio, 2001; Mace et al., 2003; Zhang and Anastasio, 2003; Mader et al., 2004), accounting for ~13% of the dissolved organic carbon in fog droplets, and ~10% of the water-soluble organic carbon in PM2.5 (Zhang and Anastasio, 2003). These amino constituents have also been hypothesized to play a role in the chemistry of fog and cloud droplets, possibly by influencing the buffering capacity and pH. In this work, we investigate the hygroscopicity of two amino acids: DL-leucine, and DL-glutamic acid.

Leucine

As shown in Figure 4.8, DL-leucine does not exhibit water uptake. Instead, the particles decreased in size upon humidification, resulting in growth factors less than unity throughout the entire range of RH studied. While loss of trapped methanol may be able to explain a decrease in particle size over a small range in RH as discussed previously, a continuous decrease such as that exhibited by DL-leucine probably cannot be attributed to evaporation alone. Thus, we speculate that this shrinkage with RH is due to structural rearrangement of the molecule upon exposure to water vapor, as previously observed for other species in other works (Weingartner et al., 1997; Mikhailov et al., 2004) and discussed earlier. The slightly higher degree of shrinkage observed for 180-nm particles compared to that of the 60-nm particles, while within the experimental uncertainty, is also consistent with observations made by Weingartner et al. (1997), in which shrinking is slightly more pronounced for larger carbon particles (wet to dry diameter ratios of 0.90 and 0.92 for 108-nm and 52-nm particles, respectively).

In the only other known hygroscopicity study of leucine, Chan et al. (2005) reported that wet L-leucine particles crystallize at 85–90% RH and that the solid particles do not absorb water even at 98%. Our observation of no hygroscopic growth is consistent with their results as well as their estimate of DRH of 99.9% (using UNIFAC). Moreover, since leucine is a six-carbon molecule that is only slightly water soluble, similar to adipic acid, it is expected that the two compounds would exhibit similarly minute water uptake. The companion study to this work also reports that DL-leucine has a similar activation diameter to adipic acid, which further reinforces this similarity. The reason that Chan et al. (2005) did not detect a similar decrease in particle size in their study could be due to two reasons. First, the nature of the particle itself could be different—their large particle is generated from the bulk form and not atomized and thus could be non-porous. Second, the reason could be due to the difference in measurement techniques. Essentially, the EDB measures the change in balancing voltage required to levitate the particle and infers the change of the particle mass from this value. Thus, if structural reorganization occurs without significant gain of water mass and a simultaneous light scattering measurement is not available, changes in particle size could go undetected in the EDB.

DL-glutamic acid monohydrate

As shown in the Table 4.1, glutamic acid is structurally similar to glutaric acid, but has an additional amine group substituent. Even though leucine and glutamic acid have similar water solubilities and not very different molecular weights, glutamic acid has been found to be completely wettable by water, while leucine is not and forms a finite contact angle with water (Raymond and Pandis, 2002). This is probably related to the additional carboxylic acid functional group in glutamic acid which makes interaction with water molecules more favorable. Thus, we would expect that glutamic acid would be more hygroscopic than leucine. Indeed, our measurement suggests that this is the case, as shown in Figure 4.9. Glutamic acid undergoes a very slight reduction in particle diameter over a limited range (10–35% RH) before the size increase due to water uptake dominates and *GF* exceeds unity. Otherwise, glutamic acid exhibits a smooth hygroscopicity curve, without a clear phase transition.

Huff Hartz et al. (2006) observed that glutamic acid holds on to water and exists in a highly supersaturated state even when held at ~5% RH for over 10 hours in their EDB study. Such lack of phase transition has also been observed (Peng et al., 2001; Chan et al., 2005) for citric acid, tartaric acid, arginine, asparagine, as well as malic acid, which will be discussed below. This high affinity for water at low RH probably explains the fact that DL-glutamic acid can only be obtained in the monohydrate form. Because the particle was not water free at low RH, the EDB results were presented as mass ratios rather than mass fraction solute as is customary. For comparison with our data, the calculation for growth factors from these mass ratios is then based on this water-containing reference phase. This is the reason their data points approach *GF* = 1 in Figure 4.9.

In order to obtain a hygroscopic growth curve that eliminates the effects of the particle shrinkage at low RH, we again rescale *GF* with respect to the diameter at maximum compaction as in the case of oxalic acid. The result is shown in Figure 4.9 to agree well with data from Huff Hartz et al. (2006). An empirical curve of the form of Eq. 4.2 is fitted through the data, and the parameters are presented in the figure and in Table 4.2.

4.4.3 Other multifunctional acids

Malic acid

Malic acid is structurally similar to succinic but has one substituted OH group. It has been identified in atmospheric aerosol and regarded as a component of SOA and an intermediate in the oxidation of unsaturated fatty acids (Sempere and Kawamura, 1994; Ion et al., 2005; Kourtchev et al., 2005). Figure 4.10 shows the hygroscopic growth curves measured for malic acid. Data form two experiments are shown (each with a fresh atomizer solution), which indicates that growth curves are quite reproducible. The 180-nm classified particles, which became 160–163 nm after evaporation, generated a *GF* curve that agrees well with both literature data and the model predictions. The 60-nm classified particles again show increased water uptake that deviates from both previous data and the model predictions. This higher uptake probably has a common cause as that for growth deviations for small phthalic acid particles.

The DRH of malic acid is measured to be 57.6–58.9% (Brooks et al., 2002; Wise et al., 2003). These measurements were performed using a bulk solution, however, and deliquescence/efflorescence behavior has never been observed in particle form. Peng et al. (2001) observed that malic acid exhibits a smooth growth curve, absorbing and desorbing water continuously and reversibly. Unlike the low-molecular weight diacids, malic acid still contains 5% residual water even when dried to 5% RH, due to strong interactions of the polar functional groups with water molecules at high supersaturations. Our results are consistent with this behavior of continuous absorption of water with RH.

2-hydroxycaproic acid

2-hydroxycaproic acid is a six-carbon carboxylic acid with an alcohol functional group. It is a potential surrogate standard for gas and liquid chromatography to quantify SOA because of the presence of these acid/alcohol moieties as well as the similar molecular weights and retention times as those of species found in SOA samples. Figure 4.12 shows that 2-hydroxycaproic acid exhibits smooth and slight water uptake, and the data from two classified sizes agree well with each other. A curve is fit through the combined data from both sizes and the parameters are reported in Table 4.2. No literature data are available for comparison with our hygroscopic growth curve. However, it is interesting to note that the curve has a similar shape and magnitude in *GF* as curves measured for SOA systems (Varutbangkul et al., 2006).

Cis-pinonic acid

Cis-pinonic acid is one of the major particle-phase oxidation products of α-pinene and β-pinene (Yu et al., 1999), which are important biogenic hydrocarbons. As shown in Figure 4.12, we observed that cis-pinonic acid exhibits a smooth water uptake curve without a deliquescence behavior. This result is different from observations of Cruz and Pandis (2000), who did not observe any hygroscopic growth of 100-nm cis-pinonic particles. The authors attributed their observation to either a pinonic acid DRH of >95% or a lower DRH accompanied by a minute amount of water that is less than the detection limit of the instrument (0.03 in GF). In our experiment, because larger classified sizes could not yield enough particles to be properly scanned by the DMA2, only the water uptake based on 60-nm classified particles is measured. We cannot entirely rule out the possibility that the pinonic acid hygroscopic growth could be an artifact of our experiment, given that two other compounds have shown unexpectedly large water uptake behavior when generated from methanol. However, the cis-pinonic acid *GF* curve shown in Figure 4.12 has a very different shape from those clearly erroneous curves of malonic acid and glutaric acid. The magnitude of *GF* calculated for pinonic acid is also within a reasonable range (GF ~1.1 at 80% RH), and is similar to *GF*s measured for SOA generated from photooxidation of a variety of biogenic monoterpenes (Varutbangkul et al., 2006). These factors suggest that the hygroscopic growth observed for pinonic acid in our experiment may be real.

Sinapic acid

Sinapic acid is a large, highly functionalized hydrocarbon (C_{11}) with a ring structure and several double bonds. It is used as a surrogate liquid chromatography standard for a compound with the molecular formula $C_{10}H_{16}NO_7S$, which has been identified as the SOA product from α-pinene photooxidation in the presence of NO_x (Gao et al., 2006). The suitability of sinapic acid as a surrogate compound is due to its biogenic nature and similar retention time in the LC as the identified compound, which was the most abundant species detected in SOA sampled in the southeastern US.

Figure 4.13 shows that sinapic acid exhibits a smooth and slight water uptake similar to that of 2-hydroxycaproic acid. Data derived from both the 60-nm and 180-nm classified sizes also match well with each other, and the curve fitting is performed using combined data from two sizes. The issues of particle shrinking at moderate RH or deviation of the water uptake curve based on the 60-nm classified diameters appear not to apply to sinapic acid or 2-hydroxycaproic acid. Also, for these two compounds, the *GF*s measured from the double-growth-column mode, in which particles traverse through two mixing columns in series resulting in a growth time of at least 91 s, are identical to those measured using only one column. Thus, the low *GF* values measured for sinapic acid and 2-hydroxycaproid acid represent water uptake at full equilibrium.

4.4.4 Fatty acids and steroid

Myristic acid, palmitic acid, and stearic acid belong to a class of long-chain fatty acids that are highly surface active but are essentially insoluble. These high-molecular weight fatty acids, along with cholesterol, have been detected in meat-cooking aerosols (Rogge et al., 1991). Stearic acid has also been identified in a mixture of compounds proposed to be photooxidation products of biogenic unsaturated fatty acids (Stephanou and Stratigakis, 1993). Figure 4.14 shows that these compounds do not uptake any water even at high RH and with the extended growth time from the double-column mode of measurement. This is consistent with the high molecular weight, very low water solubility, and only a single functional group in the long aliphatic chains for the fatty acids and the large hydrophobic ring structures for cholesterol.

4.4.5 Comparison of growth factors of different organic species

From the curves fitted to the hygroscopic growth data points of each organic compound studied, a *GF* value at a reference RH of 85% can be calculated (see Table 4.2). Figure 4.15a shows that the *GF* values anticorrelate with the pK_a of the organic species, which is intuitive since pK_a is a measure of the tendency for the organic to keep its H^+ ion from dissociating in solution. On the other hand, Figure 4.15b shows that *GF*s measured do not strongly correlate with water solubility of the organic compound as would be expected. Note that anomalous malonic acid and glutaric acid data are not fitted with Eq. 4.2; thus their *GF*s at 85% are excluded from Figure 4.15.

4.5 Conclusions

In this work, we investigate the hygroscopic behavior of pure organic aerosols of various types: dicarboxylic acids, amino acids, multifunctional acids, fatty acids, and a steroid. Particles are generated by atomizing the organic compound from a methanol solution in order to achieve water-free particles. In summary, our experiments show that succinic acid, adipic acid, high-molecular-weight fatty acids, and cholesterol do not take up a measurable amount of water when exposed to high humidity, even when allowed over 90 s of growth time. In the class of multifunctional acids, cis-pinonic acid, 2-hydroxycaproic acid, and sinapic acid all exhibit slight water uptake. The hygroscopic growth curve of each compound can be fitted with a three-parameter empirical form. DL-malic acid is more hygroscopic, and the results from our 180-nm classified particles agree well with literature data as well as the predictions made by the ADDEM model. For the amino acids, DL-leucine shows only a decrease in particle size with RH and no growth. We hypothesize that this may be due to slight structural rearrangement of a porous particle, leading to particle collapse at higher humidities. DL-glutamic acid monohydrate shows a similar behavior but for only a small range of RH, beyond which the water uptake dominates. Correction of such data is performed by rescaling *GF* with the minimum particle diameter measured. This yields a growth curve of DL-glutamic acid that is consistent with literature data.

Phthalic acid also shows moderate uptake of water, and our data from 180-nm classified particles are similar to results of previous study. However, the 60-nm classified particles of phthalic acid and DL-malic acid exhibits increased water uptake over the results of 180-nm particles, the literature values, and the model. This effect may be related to the fact that particle evaporation is suppressed by the presence of water film at higher RHs, and that smaller particles are more susceptible to the dry evaporation which occurs during verification of the classified size. Finally, for oxalic acid, the measured *GF* is comparable to literature data, but the growth cannot be reproduced by the ADDEM model. This could be due to uncertainties in the dry and liquid particle density and UNIFAC model parameters, to which the model is sensitive in the oxalic acid case.

Our results show that the species that exhibit hygroscopic growth still do so in a smooth fashion, which is normally indicative of a deliquesced particle. We do not observe any deliquescence or efflorescence behavior for any of the compounds studied, similar to the results of Prenni et al. (2001) who observed the efflorescence branch growth factors for five diacids despite drying them to 5% RH. Our growth curves also generally agree with literature data that were obtained from aqueous solutions. These observations are somewhat surprising as the particles originate from a methanol solution, and care is taken to thoroughly dry all air flows entering the system so as to introduce as little water vapor as possible before the classifying DMA. Thus, the particles should never have been exposed to even a moderate amount of water vapor before classification takes place, much less the extremely high RHs that would be necessary to deliquesce particles of many of these species. Questions remain whether methanol could be retained in the particles even after extensive drying using silica gel, molecular sieves, and Nafion dryers, and whether such trapped solvent could help induce hygroscopic behavior of the particle as if it were in solution with water. These factors may also help explain the anomalous growth behavior measured for malonic acid and glutaric acid, which appear to be caused by the methanol atomization scheme.

In light of the observations summarized above, we find that particle morphology can affect the water uptake behavior. A number of complications arise from using methanol as the atomizing solvent and mainly relate to the possibly incomplete removal of methanol from the aerosol phase. If loss of trapped methanol occurs slowly and continue in the scanning DMA, particle size measurement may be affected. Because of these issues, we recommend that future studies employ other volatile organic solvents for atomization purposes when water-free particles are desired. Less-polar solvents such as cyclohexane or dichloromethane may be less likely to solvate with the acid species and could be removed more readily from the particle phase, which may reduce some of the complications seen in these experiments. Non-polar solvents would also be beneficial in terms of not influencing the RH measurement by the hygrometer. Despite these difficulties associated with methanol, however, we find that useful data can still be obtained in our experiments after corrections for particle restructuring.

4.6 Acknowledgements

This work is funded by the Environmental Protection Agency and Department of Energy. The authors thank Chak Chan and Kirsten Koehler for providing their EDB and HTDMA data points for comparison with our work. We also thank Adam Olsen, Jesse Kroll, and Jason Surratt for helpful discussions.

4.7 References

Baxter, G. P. and Lansing, J. E.: The aqueous pressure of some hydrated crystals. Oxalic acid, strontium chloride and sodium sulfate, Journal of the American Chemical Society, 42, 419–426, 1920.

Bilde, M., Svenningsson, B., Monster, J. and Rosenorn, T.: Even-odd alternation of evaporation rates and vapor pressures of C3–C9 dicarboxylic acid aerosols, Environ. Sci. Technol., 37, 1371–1378, 2003.

Braban, C. F., Carroll, M. F., Styler, S. A. and Abbatt, J. P. D.: Phase transitions of malonic and oxalic acid aerosols, J. Phys. Chem. A, 107, 6594–6602, 2003.

Brooks, S. D., DeMott, P. J. and Kreidenweis, S. M.: Water uptake by particles containing humic materials and mixtures of humic materials with ammonium sulfate, Atmos. Environ., 38, 1859–1868, 2004.

Brooks, S. D., Garland, R. M., Wise, M. E., Prenni, A. J., Cushing, M., Hewitt, E. and Tolbert, M. A.: Phase changes in internally mixed maleic acid/ammonium sulfate aerosols, J. Geophys. Res.–Atmos., 108, art. no. 4487, doi:10.1029/2002JD003204, 2003.

Brooks, S. D., Wise, M. E., Cushing, M. and Tolbert, M. A.: Deliquescence behavior of organic/ammonium sulfate aerosol, Geophys. Res. Lett., 29, art. no. 1917, doi:10.1029/2002GL014733, 2002.

Chan, M. N. and Chan, C. K.: Hygroscopic properties of two model humic-like substances and their mixtures with inorganics of atmospheric importance, Environ. Sci. Technol., 37, 5109–5115, 2003.

Chan, M. N. and Chan, C. K.: Mass transfer effects in hygroscopic measurements of aerosol particles, Atmos. Chem. Phys., 5, 2703–2712, 2005.

Chan, M. N., Choi, M. Y., Ng, N. L. and Chan, C. K.: Hygroscopicity of water-soluble organic compounds in atmospheric aerosols: Amino acids and biomass burning derived organic species, Environ. Sci. Technol., 39, 1555–1562, 2005.

Choi, M. Y. and Chan, C. K.: Continuous measurements of the water activities of aqueous droplets of water-soluble organic compounds, J. Phys. Chem. A, 106, 4566–4572, 2002a.

Choi, M. Y. and Chan, C. K.: The effects of organic species on the hygroscopic behaviors of inorganic aerosols, Environ. Sci. Technol., 36, 2422–2428, 2002b.

Collins, D. R., Flagan, R. C. and Seinfeld, J. H.: Improved inversion of scanning DMA data, Aerosol Sci. Technol., 36, 1–9, 2002.

Cruz, C. N. and Pandis, S. N.: Deliquescence and hygroscopic growth of mixed inorganic-organic atmospheric aerosol, Environ. Sci. Technol., 34, 4313–4319, 2000.

Cziczo, D. J., Nowak, J. B., Hu, J. H. and Abbatt, J. P. D.: Infrared spectroscopy of model tropospheric aerosols as a function of relative humidity: Observation of deliquescence and crystallization, J. Geophys. Res.–Atmos., 102, 18843–18850, 1997.

Fredenslund, A., Jones, R. L. and Prausnitz, J. M.: Group-contribution estimation of activity coefficients in nonideal liquid mixtures, AIChE J., 21, 1086–1099, 1975.

Fredenslund, A. and Sorensen, J. M.: Models for thermodynamic and phase equilibria calculations, Marcel Dekker, New York, 1994.

Gamble, D. S., Underdown, A. W. and Langford, C. H.: Copper(II) titration of fulvic acid ligand sites with theoretical, potentiometric, and spectrophotometric analysis, Analytical Chemistry, 52, 1901–1908, 1980.

Gao, S., Surratt, J. D., Knipping, E. M., Edgerton, E. S., Shahgholi, M. and Seinfeld, J. H.: Characterization of polar organic components in fine aerosols in the southeastern United States: Identity, origin, and evolution, J. Geophys. Res.–Atmos, in press, 2006.

Gysel, M., Weingartner, E., Nyeki, S., Paulsen, D., Baltensperger, U., Galambos, I. and Kiss, G.: Hygroscopic properties of water-soluble matter and humic-like organics in atmospheric fine aerosol, Atmos. Chem. Phys., 4, 35–50, 2004.

Hameri, K., Charlson, R. and Hansson, H. C.: Hygroscopic properties of mixed ammonium sulfate and carboxylic acids particles, AIChE J., 48, 1309–1316, 2002.

Hansen, H. K., Rasmussen, P., Fredenslund, A., Schiller, M. and Gmehling, J.: Vapor-liquid equilibria by UNIFAC group contribution. 5. Revision and extension, Ind. Eng. Chem. Res., 30, 2352–2355, 1991.

Hansson, H. C., Wiedensohler, A., Rood, M. J. and Covert, D. S.: Experimental determination of the hygroscopic properties of organically coated aerosol particles, J. Aerosol Sci., 21, S241–S244, 1990.

Huff Hartz, K. E., Tischuk, J. E., Chan, M. N., Chan, C. K., Donahue, N. M. and Pandis, S. N.: Cloud condensation nuclei activation of limited solubility organic aerosol, Atmos. Environ., 40, 605–617, 2006.

Ion, A. C., Vermeylen, R., Kourtchev, I., Cafmeyer, J., Chi, X., Gelencser, A., Maenhaut, W. and Claeys, M.: Polar organic compounds in rural PM2.5 aerosols from K-puszta, Hungary, during a 2003 summer field campaign: Sources and diel variations, Atmos. Chem. Phys., 5, 1805–1814, 2005.

Jimenez, J. L., Bahreini, R., Cocker, D. R., Zhuang, H., Varutbangkul, V., Flagan, R. C., Seinfeld, J. H., O'Dowd, C. D. and Hoffmann, T.: New particle formation from photooxidation of diiodomethane (CH_2I_2), J. Geophys. Res.–Atmos, 108, art. no. 4318, doi:10.1029/2002JD002452, 2003.

Kawamura, K., Sempere, R., Imai, Y., Fujii, Y. and Hayashi, M.: Water soluble dicarboxylic acids and related compounds in Antarctic aerosols, J. Geophys. Res.–Atmos., 101, 18721–18728, 1996.

Kerminen, V. M., Ojanen, C., Pakkanen, T., Hillamo, R., Aurela, M. and Merilainen, J.: Low-molecular-weight dicarboxylic acids in an urban and rural atmosphere, J. Aerosol Sci., 31, 349–362, 2000.

Koehler, K. A., Kreidenweis, S. M., DeMott, P. J., Prenni, A. J., Carrico, C. M., Ervens, B. and Feingold, G.: Water activity and activation diameters from hygroscopicity data—part II: Application to organic species, Atmos. Chem. Phys., 6, 795–809, 2006.

Kourtchev, I., Ruuskanen, T., Maenhaut, W., Kulmala, M. and Claeys, M.: Observation of 2-methyltetrols and related photo-oxidation products of isoprene in boreal forest aerosols from Hyytiala, Finland, Atmos. Chem. Phys., 5, 2761–2770, 2005.

Lide, D. R., Ed.: CRC handbook of chemistry and physics, 84th edition, CRC Press, Florida, 2003.

Liu, B. Y. H., Pui, D. Y. H., Whitby, K. T., Kittelson, D. B., Kousaka, Y. and McKenzie, R. L.: Aerosol mobility chromatograph—new detector for sulfuric acid aerosols, Atmos. Environ., 12, 99–104, 1978.

Mace, K. A., Artaxo, P. and Duce, R. A.: Water-soluble organic nitrogen in amazon basin aerosols during the dry (biomass burning) and wet seasons, J. Geophys. Res.–Atmos., 108, art no. 4512, doi:10.1029/2003JD003557, 2003.

Mader, B. T., Yu, J. Z., Xu, J. H., Li, Q. F., Wu, W. S., Flagan, R. C. and Seinfeld, J. H.: Molecular composition of the water-soluble fraction of atmospheric carbonaceous aerosols collected during ACE-Asia, J. Geophys. Res.–Atmos., 109, D06206, doi:10.1029/2003JD004105, 2004.

McMurry, P. H. and Stolzenburg, M. R.: On the sensitivity of particle size to relative humidity for Los Angeles aerosols, Atmos. Environ., 23, 497–507, 1989.

Mikhailov, E., Vlasenko, S., Niessner, R. and Poschl, U.: Interaction of aerosol particles composed of protein and salts with water vapor: Hygroscopic growth and microstructural rearrangement, Atmos. Chem. Phys., 4, 323–350, 2004.

Mikhailov, E. F., Vlasenko, S. S., Podgorny, I. A., Ramanathan, V. and Corrigan, C. E.: Optical properties of soot–water drop agglomerates: An experimental study, J. Geophys. Res.–Atmos., 111, art. no. D07209, doi:10.1029/2005JD006389, 2006.

Ming, Y. and Russell, L. M.: Thermodynamic equilibrium of organic-electrolyte mixtures in aerosol particles, AIChE J., 48, 1331–1348, 2002.

Nenes, A., Pandis, S. N. and Pilinis, C.: ISORROPIA: A new thermodynamic equilibrium model for multiphase multicomponent inorganic aerosols, Aquat. Geochem., 4, 123–152, 1998.

Parsons, M. T., Mak, J., Lipetz, S. R. and Bertram, A. K.: Deliquescence of malonic, succinic, glutaric, and adipic acid particles, J. Geophys. Res.–Atmos., 109, art. no. D06212, doi:10.1029/2003JD004075, 2004.

Peng, C., Chan, M. N. and Chan, C. K.: The hygroscopic properties of dicarboxylic and multifunctional acids: Measurements and UNIFAC predictions, Environ. Sci. Technol., 35, 4495–4501, 2001.

Peng, C. G. and Chan, C. K.: The water cycles of water-soluble organic salts of atmospheric importance, Atmos. Environ., 35, 1183–1192, 2001.

Prenni, A. J., De Mott, P. J. and Kreidenweis, S. M.: Water uptake of internally mixed particles containing ammonium sulfate and dicarboxylic acids, Atmos. Environ., 37, 4243–4251, 2003.

Prenni, A. J., DeMott, P. J., Kreidenweis, S. M., Sherman, D. E., Russell, L. M. and Ming, Y.: The effects of low molecular weight dicarboxylic acids on cloud formation, J. Phys. Chem. A, 105, 11240–11248, 2001.

Rader, D. J. and McMurry, P. H.: Application of the tandem differential mobility analyzer to studies of droplet growth or evaporation, J. Aerosol Sci., 17, 771–787, 1986.

Ray, J. and McDow, S. R.: Dicarboxylic acid concentration trends and sampling artifacts, Atmos. Environ., 39, 7906–7919, 2005.

Raymond, T. M. and Pandis, S. N.: Cloud activation of single-component organic aerosol particles, J. Geophys. Res.–Atmos, 107, art. no. 4787, doi:10.1029/2002JD002159, 2002.

Rogge, W. F., Hildemann, L. M., Mazurek, M. A., Cass, G. R. and Simonelt, B. R. T.: Sources of fine organic aerosol 1. Charbroilers and meat cooking operations, Environ. Sci. Technol., 25, 1112–1125, 1991.

Rohrl, A. and Lammel, G.: Low molecular weight dicarboxylic acids and glyoxylic acid: Seasonal and air mass characteristics, Environ. Sci. Technol., 35, 95–101, 2001.

Saxena, P. and Hildemann, L. M.: Water-soluble organics in atmospheric particles: A critical review of the literature and application of thermodynamics to identify candidate compounds, J. Atmos. Chem., 24, 57–109, 1996.

Saxena, P. and Hildemann, L. M.: Water absorption by organics: Survey of laboratory evidence and evaluation of UNIFAC for estimating water activity, Environ. Sci. Technol., 31, 3318–3324, 1997.

Saxena, P., Hildemann, L. M., McMurry, P. H. and Seinfeld, J. H.: Organics alter hygroscopic behavior of atmospheric particles, J. Geophys. Res.–Atmos., 100, 18755–18770, 1995.

Scheller, E.: Amino acids in dew—origin and seasonal variation, Atmos. Environ., 35, 2179–2192, 2001.

Sempere, R. and Kawamura, K.: Comparative distributions of dicarboxylic acids and related polar compounds in snow rain and aerosols from urban atmosphere, Atmos. Environ., 28, 449–459, 1994.

Sempere, R. and Kawamura, K.: Low molecular weight dicarboxylic acids and related polar compounds in the remote marine rain samples collected from Western Pacific, Atmos. Environ., 30, 1609–1619, 1996.

Stephanou, E. G. and Stratigakis, N.: Oxocarboxylic and alpha,omega-dicarboxylic acids—photooxidation products of biogenic unsaturated fatty acids present in urban aerosols, Environ. Sci. Technol., 27, 1403–1407, 1993.

Suarez, J. T., Torresmarchal, C. and Rasmussen, P.: Prediction of surface tensions of nonelectrolyte solutions, Chemical Engineering Science, 44, 782–786, 1989.

Tamura, M., Kurata, M. and Odani, H.: Practical method for estimating surface tensions of solutions, Bulletin of the Chemical Society of Japan, 28, 83–88, 1955.

Tang, I. N.: Thermodynamic and optical properties of mixed-salt aerosols of atmospheric importance, J. Geophys. Res.–Atmos., 102, 1883–1893, 1997.

Tang, I. N. and Munkelwitz, H. R.: Water activities, densities, and refractive indexes of aqueous sulfates and sodium nitrate droplets of atmospheric importance, J. Geophys. Res.–Atmos., 99, 18801–18808, 1994.

Tao, Y. and McMurry, P. H.: Vapor pressures and surface free energies of C14–C18 monocarboxylic acids and C5-dicarboxylic and C6-dicarboxylic acids, Environ. Sci. Technol., 23, 1519–1523, 1989.

Topping, D. O., McFiggans, G. B. and Coe, H.: A curved multi-component aerosol hygroscopicity model framework: Part 1—inorganic compounds, Atmos. Chem. Phys., 5, 1205–1222, 2005a.

Topping, D. O., McFiggans, G. B. and Coe, H.: A curved multi-component aerosol hygroscopicity model framework: Part 2—including organic compounds, Atmos. Chem. Phys., 5, 1223–1242, 2005b.

Varutbangkul, V., Brechtel, F. J., Bahreini, R., Ng, N. L., Keywood, M. D., Kroll, J. H., Flagan, R. C., Seinfeld, J. H., Lee, A. and Goldstein, A. H.: Hygroscopicity of secondary organic aerosols formed by oxidation of cycloalkenes, monoterpenes, sesquiterpenes, and related compounds, Atmos. Chem. Phys. Disc., 6, 1121–1177, 2006.

Weast, R. C. and Astle, M. J., Eds.: CRC handbook of chemistry and physics, CRC Press Inc, Boca Raton, FL, 1981.

Weast, R. C. and Astle, M. J., Eds.: CRC handbook of data on organic compounds, CRC Press, Florida, 1985.

Weingartner, E., Burtscher, H. and Baltensperger, U.: Hygroscopic properties of carbon and diesel soot particles, Atmos. Environ., 31, 2311–2327, 1997.

Wise, M. E., Surratt, J. D., Curtis, D. B., Shilling, J. E. and Tolbert, M. A.: Hygroscopic growth of ammonium sulfate/dicarboxylic acids, J. Geophys. Res.–Atmos., 108, art. no. 4638, doi:10.1029/2003JD003775, 2003.

Yu, J. Z., Cocker, D. R., Griffin, R. J., Flagan, R. C. and Seinfeld, J. H.: Gas-phase ozone oxidation of monoterpenes: Gaseous and particulate products, Journal of Atmospheric Chemistry, 34, 207–258, 1999.

Zhang, Q. and Anastasio, C.: Chemistry of fog waters in California's central valley—part 3: Concentrations and speciation of organic and inorganic nitrogen, Atmos. Environ., 35, 5629–5643, 2001.

Zhang, Q. and Anastasio, C.: Free and combined amino compounds in atmospheric fine particles (pm2.5) and fog waters from northern California, Atmos. Environ., 37, 2247–2258, 2003.

Zhang, Q., Anastasio, C. and Jimemez-Cruz, M.: Water-soluble organic nitrogen in atmospheric fine particles (PM2.5) from northern California, J. Geophys. Res.–Atmos., 107, art. no. 4112, 10.1029/2001JD000870, 2002.

Table 4.1. Organic species studied (all chemicals are supplied by Sigma-Aldrich)

Organic compound	Molecular structure	Molecular formula	Molecular Weight (g/mol)	Density[a] (g/cm^3)	Solubility (g solute /cm^3 H_2O)	Dissociation Constants, pK_{a1} (pK_{ai})[c]	Vapor Pressure (Torr)[e]	Reported Purity
Dicarboxylic acids								
Oxalic acid	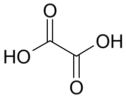	$C_2H_2O_4$	90.04	1.900	0.0951[b]	1.23[d]	2.51 x 10^{-6} 3.5 x 10^{-5} [f]	≥99%
Malonic acid	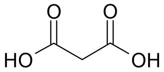	$C_3H_4O_4$	104.07	1.619	0.424[b]	2.83[d]	1.0 x 10^{-5} [f] 3.6x10^{-4} [h]	99%
Succinic acid	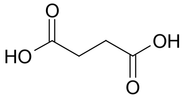	$C_4H_6O_4$	118.09	1.572	0.0835[b] (25 °C)	4.22	6.9 x 10^{-7} [f] 3.9 x 10^{-5} [h]	≥99%
Glutaric acid	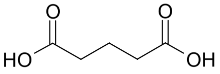	$C_5H_8O_4$	132.12	1.429	0.583[b] (25 °C)	4.35	2.23 x 10^{-4} 4.1 x 10^{-6} [f] 6.7 x 10^{-4} [h] 7.7 x 10^{-4} [i]	99%
Adipic acid	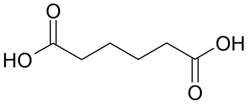	$C_6H_{10}O_4$	146.14	1.360	0.015[b] (15 °C)	4.44	1.81 x 10^{-5} 1.5 x 10^{-7} [f] 9.8 x 10^{-6} [h] 1.0 x 10^{-5} [i]	≥99%
Phthalic acid	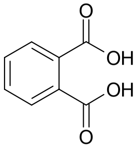	$C_8H_6O_4$	166.17	2.180	0.00697[b] (25 °C)	2.95	2.14 x 10^{-6}	≥99.5%
Amino acids								
DL-glutamic acid monohydrate	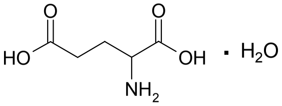	$C_5H_9NO_4 \cdot H_2O$	165.15	1.409[e]	0.0235[b] (25 °C)	9.66[a]	–	99%
DL-leucine	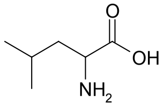	$C_6H_{13}NO_2$	131.17	1.293	0.022[b]	2.328[d]	0.0309	≥99%

Table 4.1. (continued)

Organic compound	Molecular structure	Molecular formula	Molecular Weight (g/mol)	Density[a] (g/cm^3)	Solubility (g solute /cm^3 H_2O)	Dissociation Constants, pK_{a1} (pK_{ai})[c]	Vapor Pressure (Torr)[e]	Reported Purity
			Other multifunctional acids					
DL-malic acid	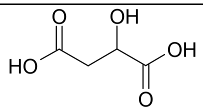	$C_4H_6O_5$	134.09	1.601[d]	1.44[b]	3.40[d]	7.19 x 10^{-5}	≥99%
2-hydroxycaproic acid	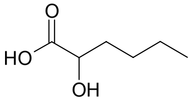	$C_6H_{12}O_3$	132.16	1.100[e]	0.032[e]	3.86[e]	9.28 x 10^{-4}	98%
cis-pinonic acid	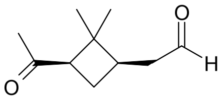	$C_{10}H_{16}O_3$	184.24	0.786[g]	0.006[g]	4.72[e]	< 10^{-5} [g]	98%
sinapic acid	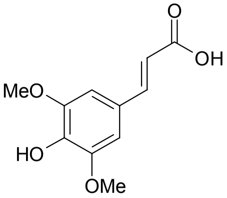	$C_{11}H_{12}O_5$	224.21	1.307[e]	0.0038[e]	3.98[e]	3.12 x 10^{-7}	98%
			Fatty acids & steroid					
myristic acid	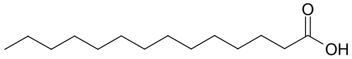	$C_{14}H_{28}O_2$	228.38	0.862	2.0 x 10^{-5} [b]	4.78[e]	1.39 x 10^{-4}	≥99.5%
palmitic acid	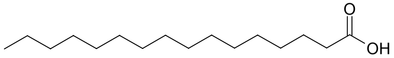	$C_{16}H_{32}O_2$	256.43	0.853	7.2 x 10^{-6} [b]	4.78	3.28 x 10^{-5}	99%
stearic acid	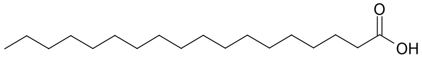	$C_{18}H_{36}O_2$	284.48	0.941	2.9 x 10^{-6} [b]	4.78	8.58 x 10^{-6}	≥98%
cholesterol	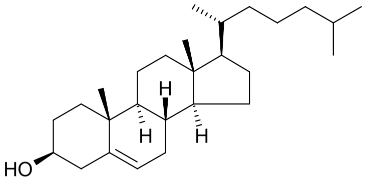	$C_{27}H_{46}O$	386.66	1.067	<3.87 x 10^{-7} [b]	15.03[e]	2.95 x 10^{-11}	≥99%

a: From *CRC Handbook*, unless specified otherwise

b: From *CRC Handbook of Data on Organic Compounds*; solubility at $T = 20$ °C, unless specified otherwise.

c: From *Dictionary of Organic Compound*; values are at $T = 25$ °C for water solutions; solubility is given at $T = 100$ °C.

d: From *Properties of Organic Compounds*; values are at $T = 25$ °C.

e: Calculated using Advanced Chemistry (ACD/Labs) Software V8.14 for Solaris (© 1994-2006 ACD/Labs) by SciFinder; $T = 25$ °C.

f: From *Prenni et al.* (2001), calculated from various sources at $T = 30$ °C.

g: From *Cruz and Pandis* (2000).

h: From *Bilde et al.* (2003), vapor pressures are at $T = 23$ °C.

i: From *Tao and McMurry* (1989).

Table 4.2. Experimental summary, curve fitting results of the final hygroscopic growth curve, and *GF* at 85% RH calculated from the fit curve for each organic compound studied

Compound	T (°C)	Fit Parameters for Eq. 4.2: $GF = 1+[(1-(RH/100))^{A} * B * (RH/100)^{C}]$			GF at 85% RH (calculated from fit)	Classified D_p after shrinking from two original D_p		% shrinkage $= \Delta D_p / D_{p,original}$	
		A	B	C		60 nm	180 nm	60 nm	180 nm
oxalic acid	25.8	0	0.53135	4.9105	1.239	43.8	-	27%	-
malonic acid	25.5	N/A [b]	N/A [b]	N/A [b]	N/A [b]	188 (from 400 nm)		47%	
succinic acid	25.3	N/A [a]	N/A [a]	N/A [a]	0	57	177	5%	2%
glutaric acid	25.6	N/A [b]	N/A [b]	N/A [b]	N/A [b]	225/334 (from 400 nm)		44% / 17%	
adipic acid	25.3	N/A [a]	N/A [a]	N/A [a]	0	59	179	2%	1%
phthalic acid	25.6	0	0.25045	2.5796	1.165	47	154	22%	14%
DL-leucine	25.5	N/A [c]	N/A [c]	N/A [c]	N/A [c]	59	176	2%	2%
DL-glutamic acid monohydrate	24.7	0.3508	0.24197	3.0549	1.076	58	-	3%	-
DL-malic acid	26.0	0.53574	0.17058	1.17	1.051	48	163	20%	9%
2-hydroxycaproic acid	25.5	0	0.12621	2.1612	1.089	52	157	13%	13%
cis-pinonic acid	25.8	0.19097	0.17712	4.2931	1.061	27	-	55%	-
sinapic acid	25.8	0	0.16028	4.2403	1.080	57	176	5%	2%
myristic acid	25.9	N/A [a]	N/A [a]	N/A [a]	0	-	150	-	17%
palmitic acid	26.6	N/A [a]	N/A [a]	N/A [a]	0	51	174	15%	3%
stearic acid	25.9	N/A [a]	N/A [a]	N/A [a]	0	58	177	3%	2%
cholesterol	25.4	N/A [a]	N/A [a]	N/A [a]	0	60	178	0%	1%

a: No hygroscopic growth is observed for this species through out the RH range studied.
b: A fit is not performed due to anomalous data. See text for detail.
c: Only particle shrinkage with humidity is observed for DL-leucine.

Table 4.3. Growth factor predictions by the ADDEM model given various input combinations of UNIFAC parameters, surface tension models, and dry and liquid density parameters for oxalic acid (courtesy of D. O. Topping and G. B. McFiggans)

Dry diameter (nm)	Revised UNIFAC parameters	Dry density [a]	Liquid density	Surface tension model (see text for details)		
				S1	S2	S3
100	Hansen et al. (1991)	Anhydrous	Dihydrate	1.599	1.600	1.594
100	Hansen et al. (1991)	Dihydrate	Dihydrate	1.525	1.526	1.520
100	Peng et al. (2001)	Anhydrous	Dihydrate	1.690	1.691	1.686
100	Peng et al. (2001)	Dihydrate	Dihydrate	1.612	1.613	1.608
50	Hansen et al. (1991)	Anhydrous	Dihydrate	1.570	1.571	1.561
50	Hansen et al. (1991)	Dihydrate	Dihydrate	1.496	1.498	1.488
50	Peng et al. (2001)	Anhydrous	Dihydrate	1.662	1.663	1.654
50	Peng et al. (2001)	Dihydrate	Dihydrate	1.584	1.585	1.576
50	Hansen et al. (1991)	Anhydrous	Anhydrous	1.551	1.552	1.542
50	Hansen et al. (1991)	Anhydrous	Dihydrate	1.570	1.571	1.561
50	Hansen et al. (1991)	Anhydrous	Water	1.660	1.661	1.651
50	Hansen et al. (1991)	Dihydrate	Anhydrous	1.478	1.479	1.469
50	Hansen et al. (1991)	Dihydrate	Dihydrate	1.496	1.498	1.488
50	Hansen et al. (1991)	Dihydrate	Water	1.582	1.583	1.574

a: Oxalic acid anhydrous density = 1.9 g/cm^3 (Perry's Chemical Engineers' Handbook)
Oxalic acid dihydrate density = 1.653 g/cm^3 (Weast and Astle, 1981)

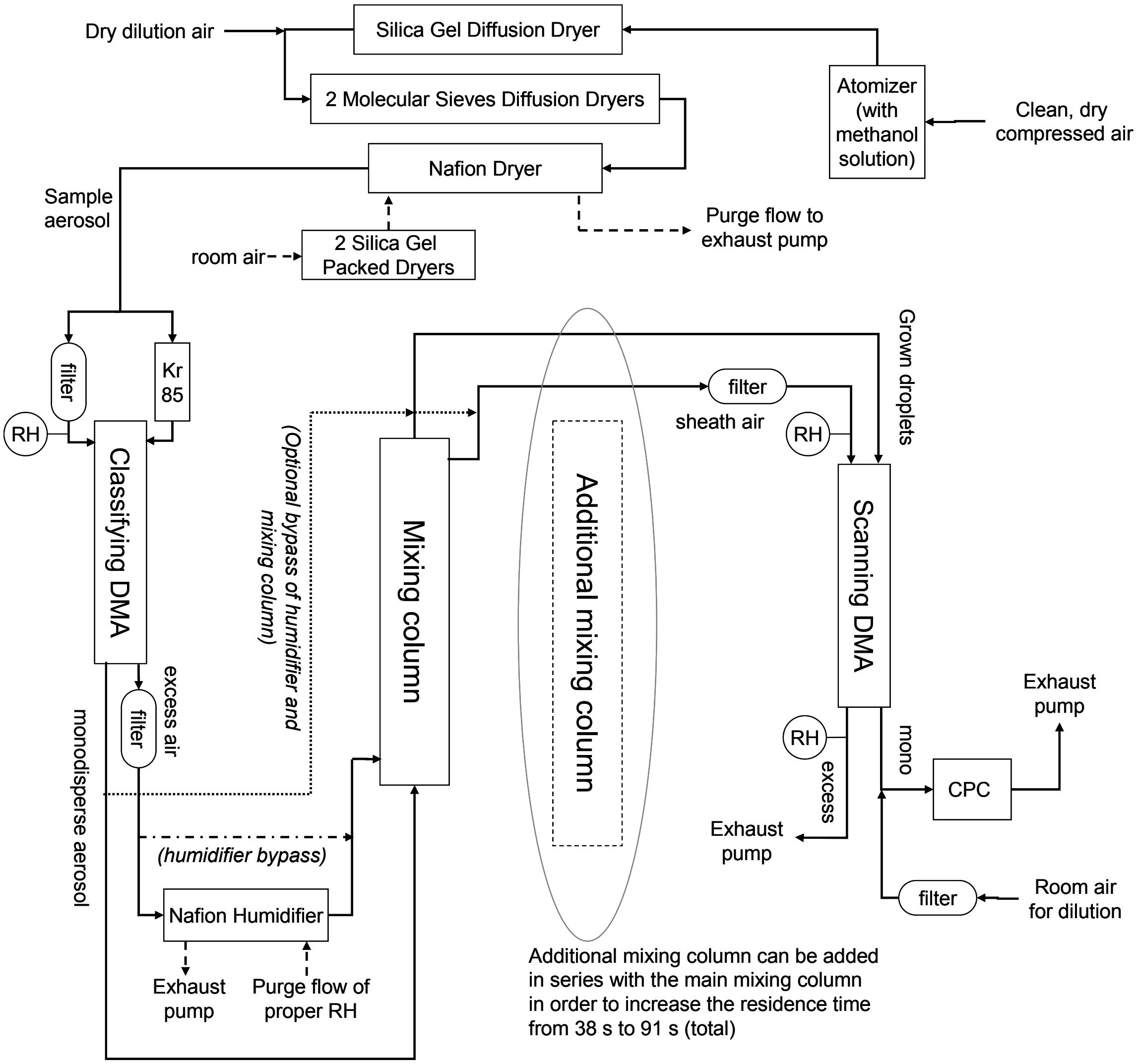

Figure 4.1. Schematic of the HTDMA system used (see text for full description).

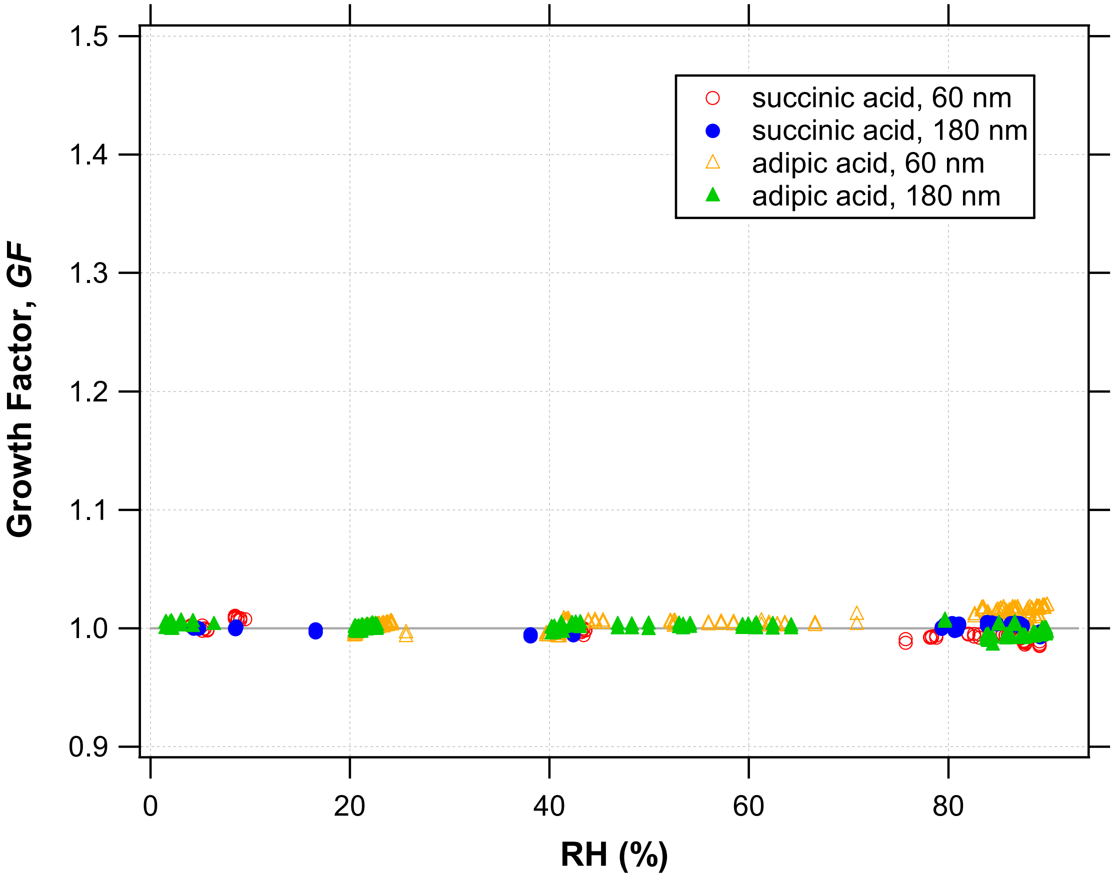

Figure 4.2. Hygroscopic growth curves for succinic acid and adipic acid. These low-solubility acids do not take up any appreciable amount of water. This is consistent with the very high deliquescent relative humidities (DRH) measured and predicted in previous studies of 98–100% RH.

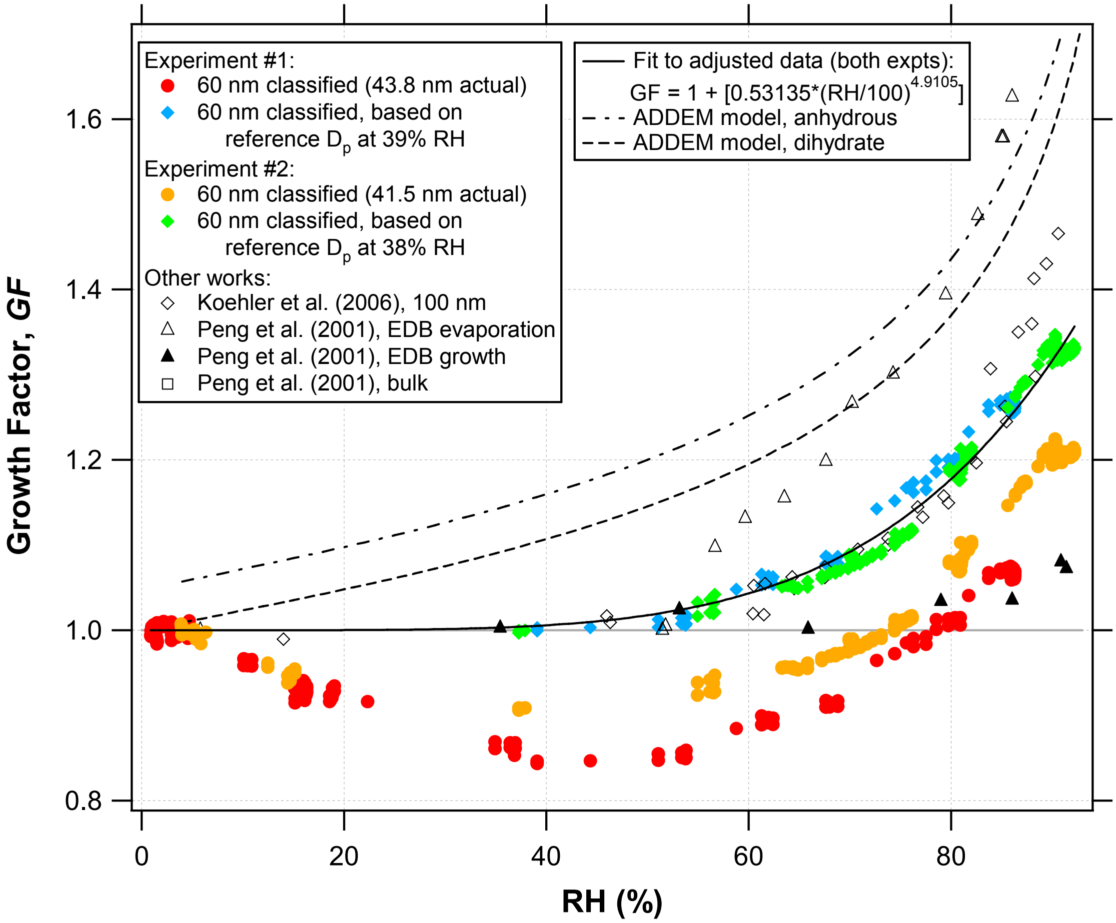

Figure 4.3. Hygroscopic growth curve for oxalic acid. Results from previous measurements indicate a large scatter, possibly an effect of the particle state and humidity history. Our experimental data showed significant decrease in size, possibly due to particle compaction or loss of trapped methanol upon particle dissolution, at low humidities before water uptake dominates. This reduction in particle size was not detected in previous work and could be specific to our experimental setup. Nevertheless, the growth factors can be adjusted using the particle diameter measured at ~40% (maximum compaction) as the reference "dry" diameter. The light blue and green diamonds represent these adjusted growth factors of the data from two experiments performed. Because the inherent assumption in this correction is that the particle contains negligible amount of water at the new reference RH the adjusted growth factors represent a lower bound of the true values. In general, our adjusted data lie closely to results of Koehler et al. (2006). None of the experimental data seem to behave similarly to model predictions, however (see text for discussion).

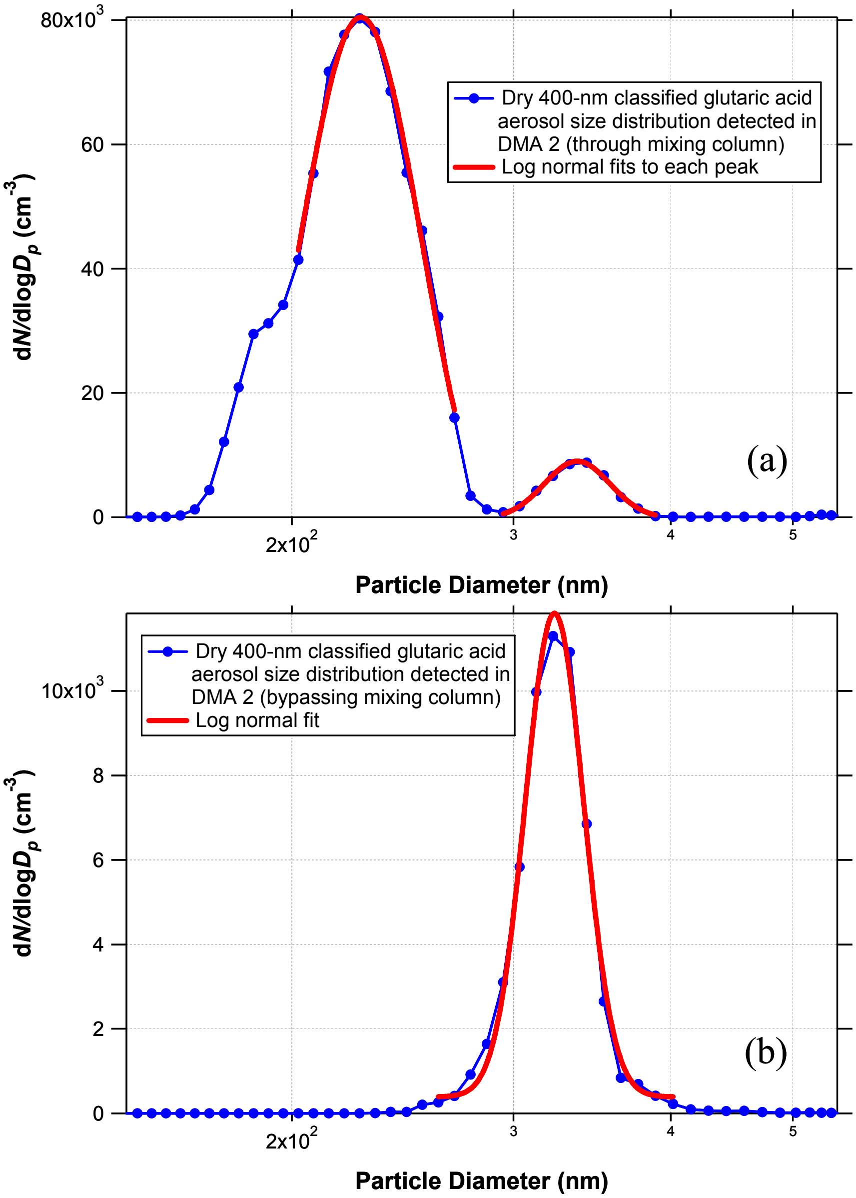

Figure 4.4. Aerosol size distributions detected by the scanning DMA of dry 400-nm classified glutaric acid particles. (a) When the particles have flowed through the mixing column, there is considerable amount of material loss, probably due to evaporation of glutaric acid itself or of remaining methanol. The distribution is approximate bimodal, with clear mode diameters of 225 nm and 334 nm. (b) If the particles are allowed to bypass the mixing column, the evaporative loss is less, and resulting peak is at ~323 nm. This indicates that at the bottom of the mixing column, when the dry particles are allowed to mix with humidified air, the size distribution is likely to be more similar to the larger-diameter mode in panel (a).

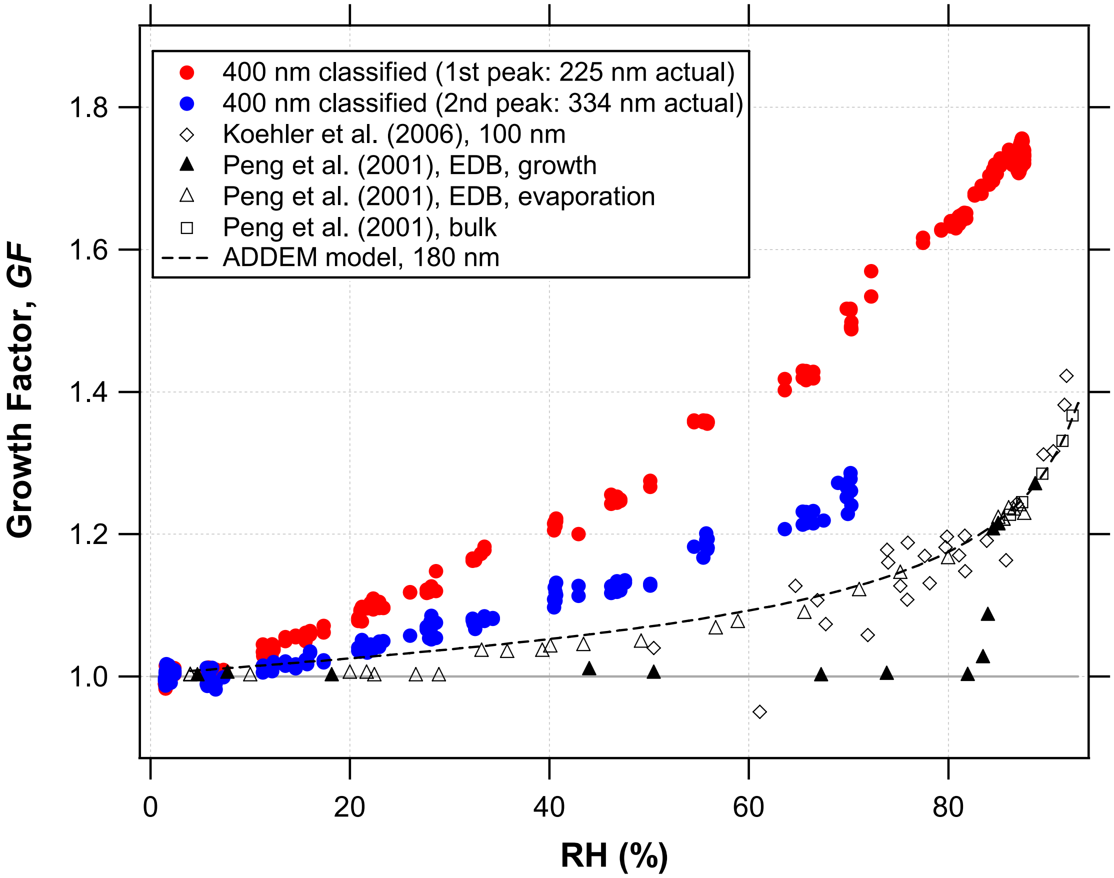

Figure 4.5. Hygroscopic growth curves for glutaric acid, calculated from the smaller-mode peak and the larger-mode peak as shown in Figure 4.4. Neither curve lies close to literature data or model prediction. This could be due to methanol's role in suppressing particle evaporation when a water film is also present. Such phenomenon could result in an RH-dependent "dry diameter" on which the growth factor calculation is based.

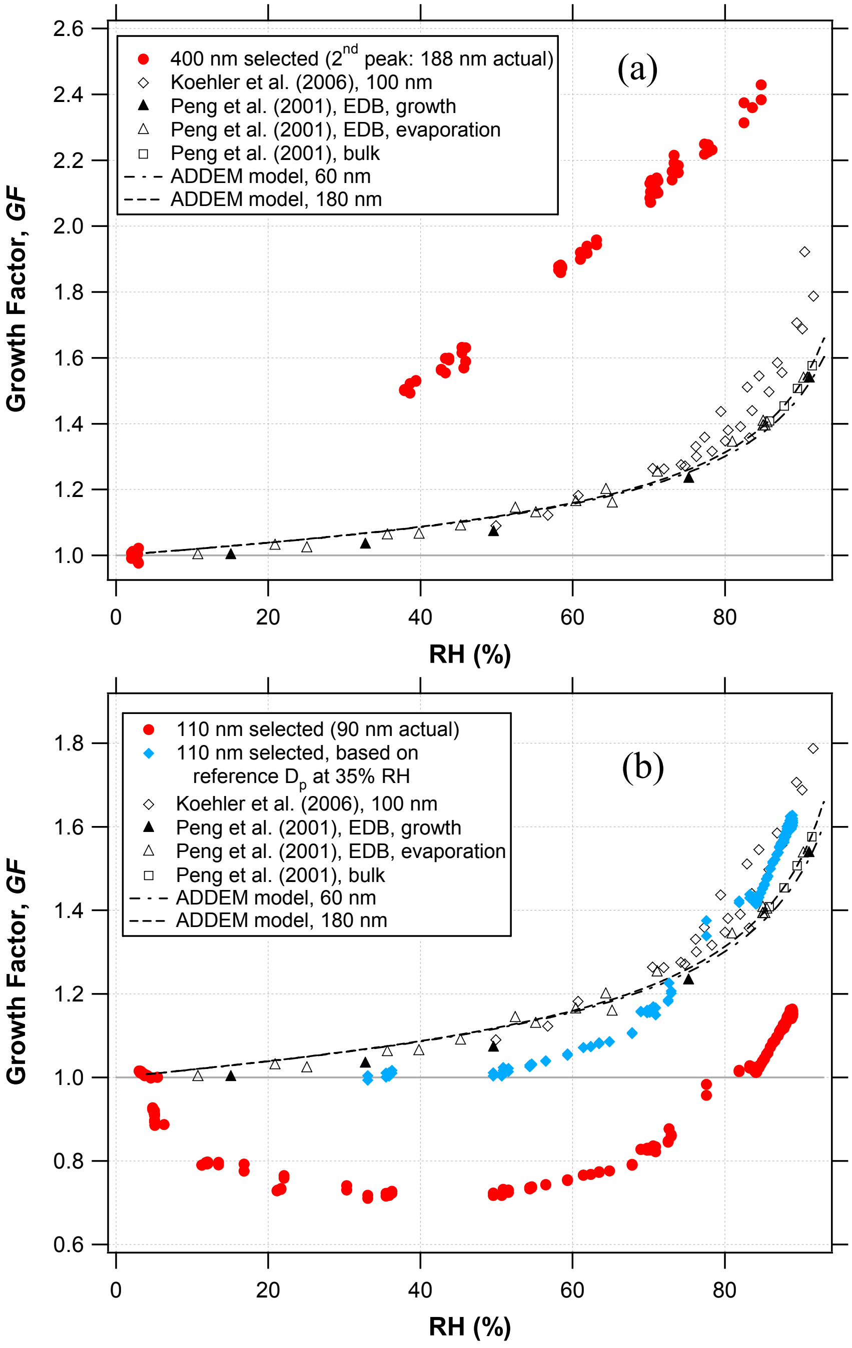

Figure 4.6. Hygroscopic growth curves for malonic acid aerosol generated from (a) a methanol solution and (b) an aqueous solution. Possible reasons for this methanol-specific anomalous growth behavior are discussed in the text.

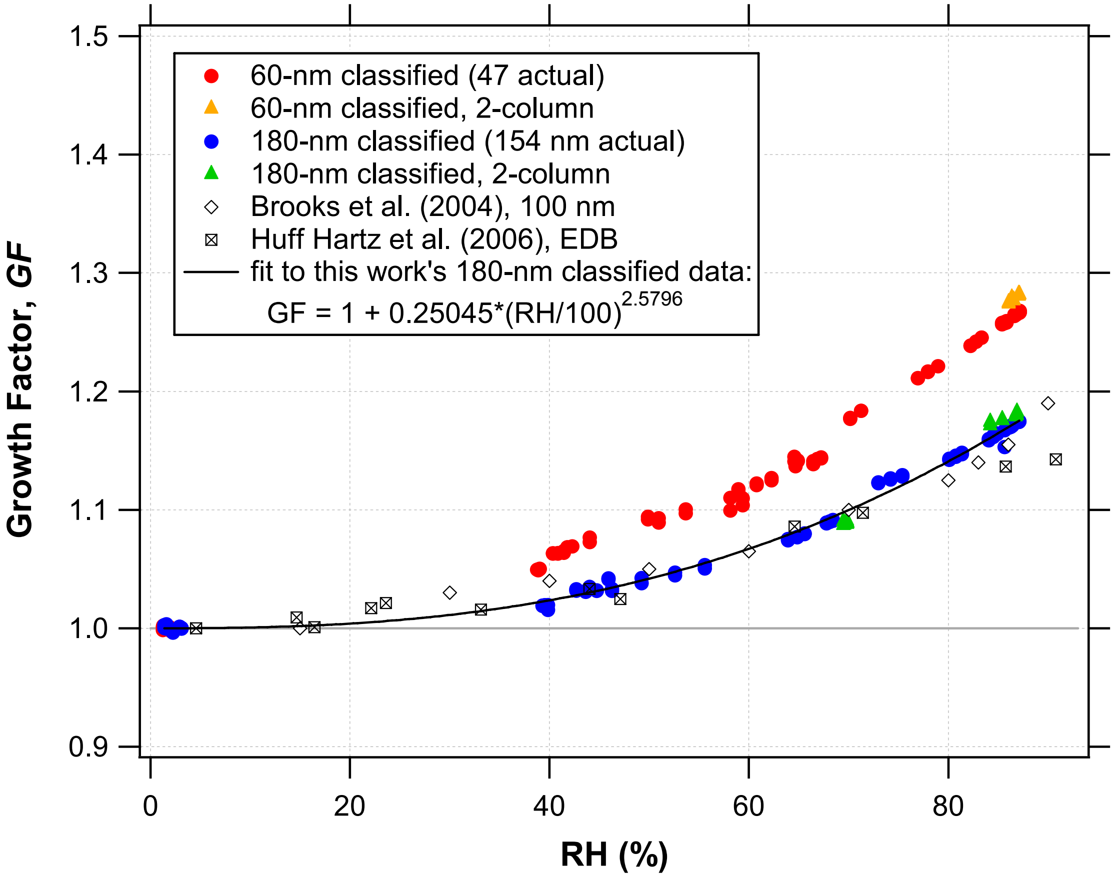

Figure 4.7. Hygroscopic growth curve of phthalic acid, compared with data points from HTDMA study of Brooks et al. (2004) and EDB study of Huff Hartz et al. (2006). Our 180-nm classified particles agree well with previous studies, while 60-nm classified particles take up more water than the 180-nm classified particles. This slightly higher water uptake could be due to suppression of particle evaporation with water, which would have a larger effect on the small particles that are more prone to evaporation in the first place. The result of underestimating the dry size of such small particles is overestimating the growth factor.

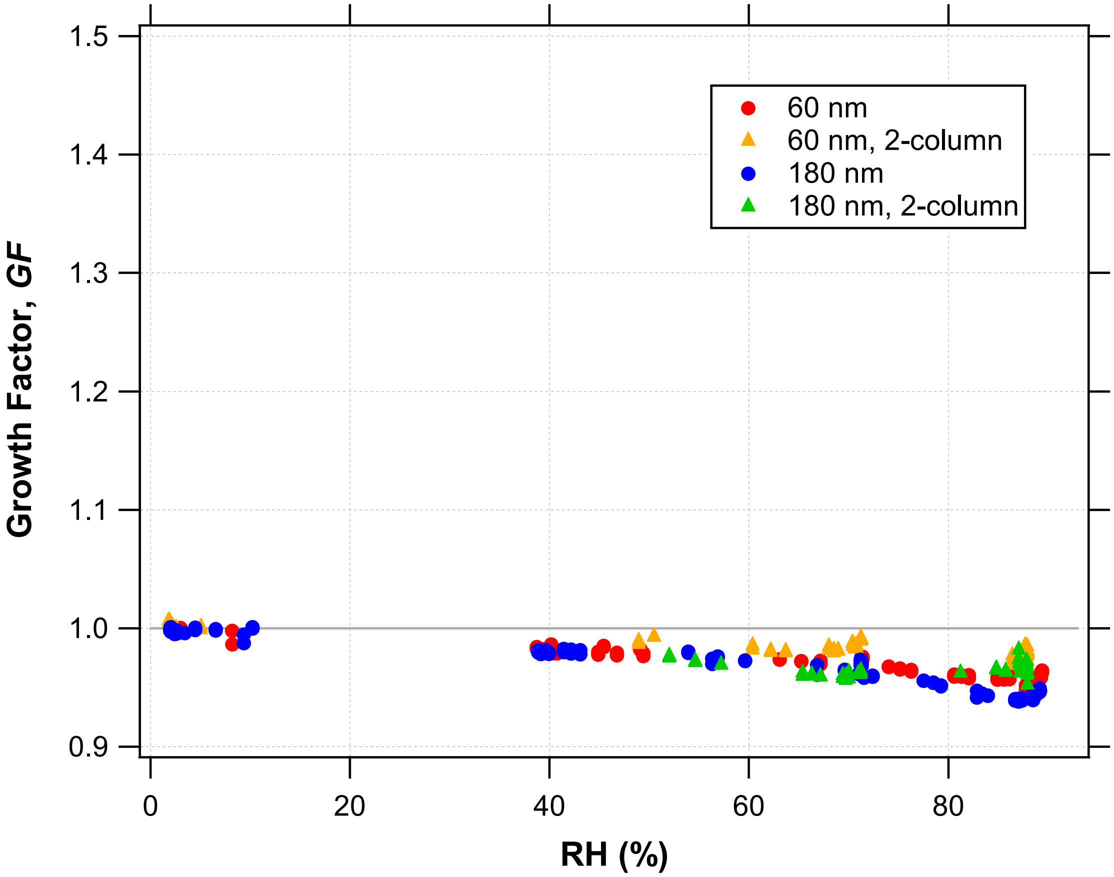

Figure 4.8. Hygroscopic growth curve of DL-leucine. The DL-leucine particles did not increase in size after humidification. Instead, they decreased in size, possibly due to structural rearrangement induced by water vapor diffusing into void volumes of porous particles.

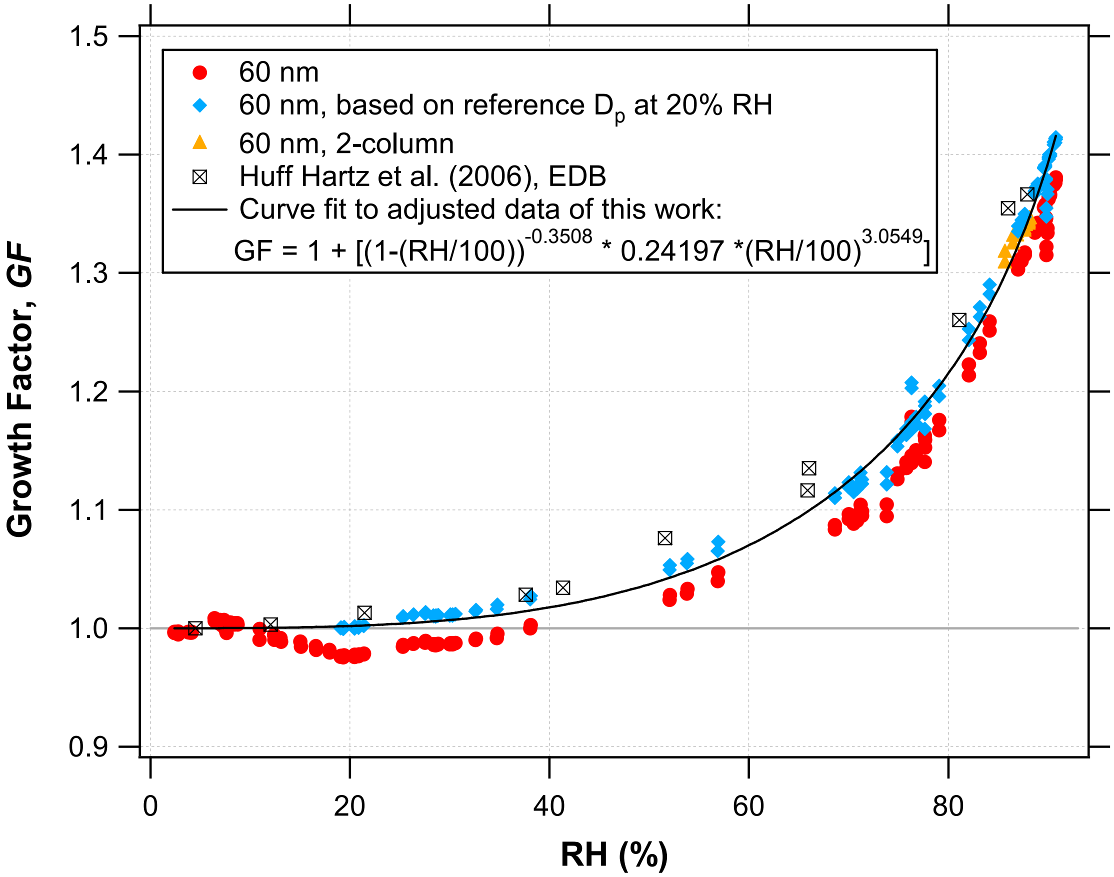

Figure 4.9. Hygroscopic growth curve of DL-glutamic acid monohydrate shows slight compaction at low humidities before water uptake dominates. The light blue diamonds represent the adjusted growth factors using the particle diameter measured at 20% (maximum compaction) as the reference "dry" diameter.

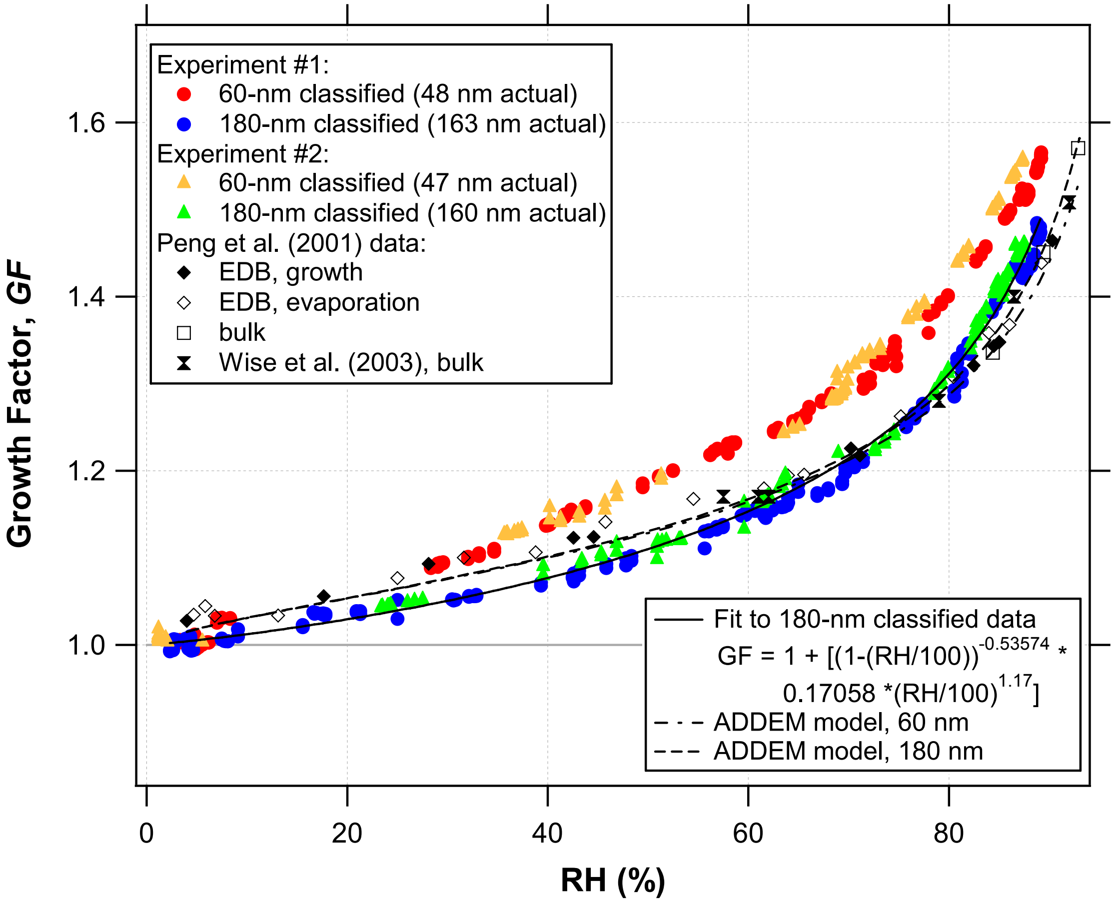

Figure 4.10. Hygroscopic growth curve for DL-malic acid. The growth curve of the 180-nm classified particles agrees well with literature data as well as the ADDEM model predictions. The 60-nm particles exhibit a slightly higher water uptake, which is probably caused by the same artifact as in the case of 60-nm classified particles of phthalic acid. Data from two experiments are plotted, showing that the results are reproducible.

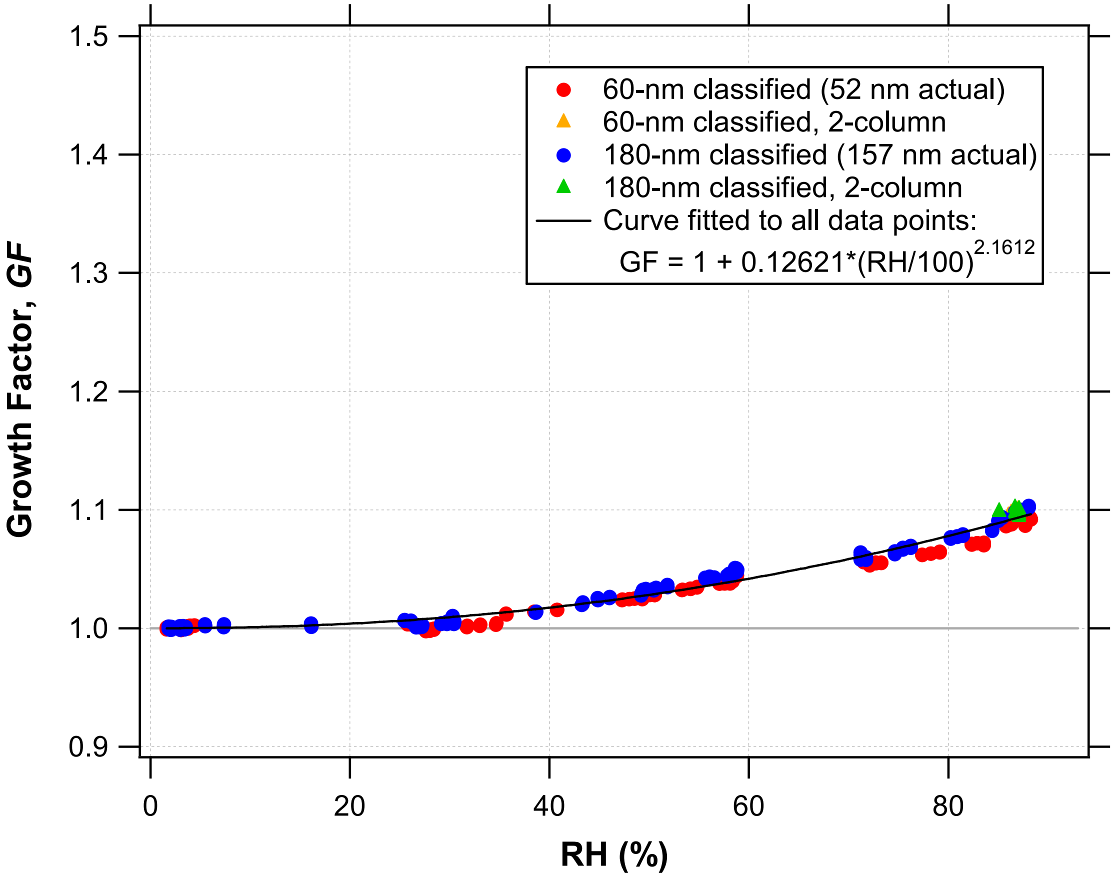

Figure 4.11. Hygroscopic growth curve for 2-hydroxycaproic acid shows slight water uptake. Results from the two classified sizes agree well with each other. *GF*s measured in the two-column mode in which particles are allotted over 90 s to grow are identical to the *GF*s measured with only one mixing column at the same RH, suggesting that the low water uptake already represents equilibrium uptake.

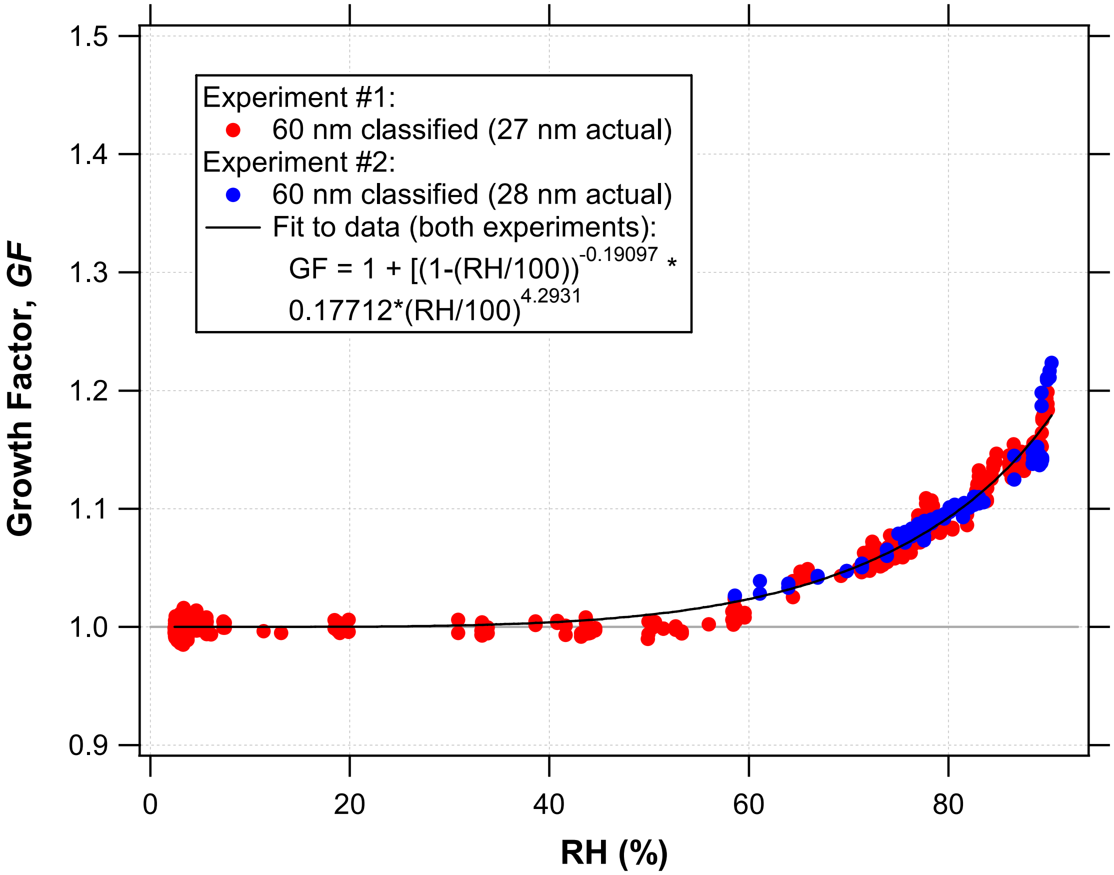

Figure 4.12. Hygroscopic growth curve for cis-pinonic acid shows slight water uptake at RH over 55%, which was not observed in previous study by Cruz and Pandis (2000).

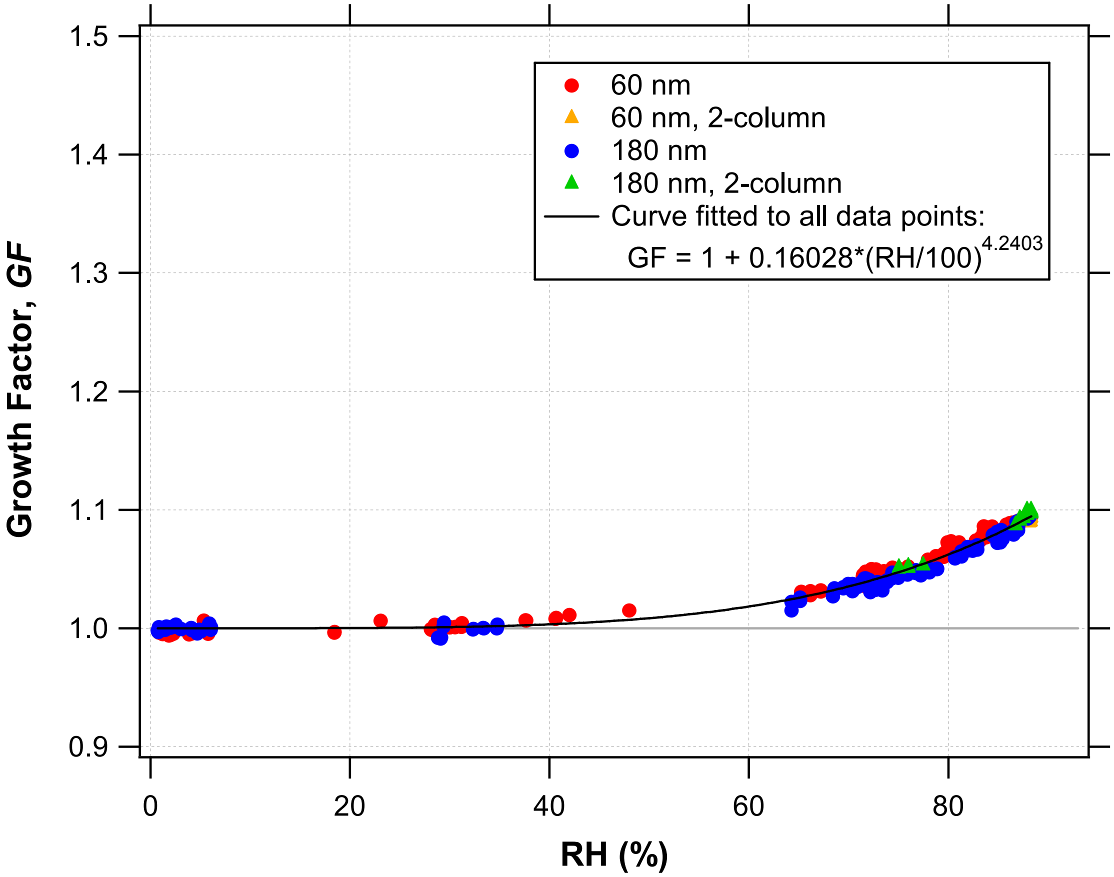

Figure 4.13. Hygroscopic growth curve of sinapic acid. As is the case for 2-hydroxycaproid acid, results from the two classified sizes agree well with each other. *GF*s measured in the two-column mode are identical to those measured with only one mixing column at the same RH, suggesting that the low water uptake already represents equilibrium uptake.

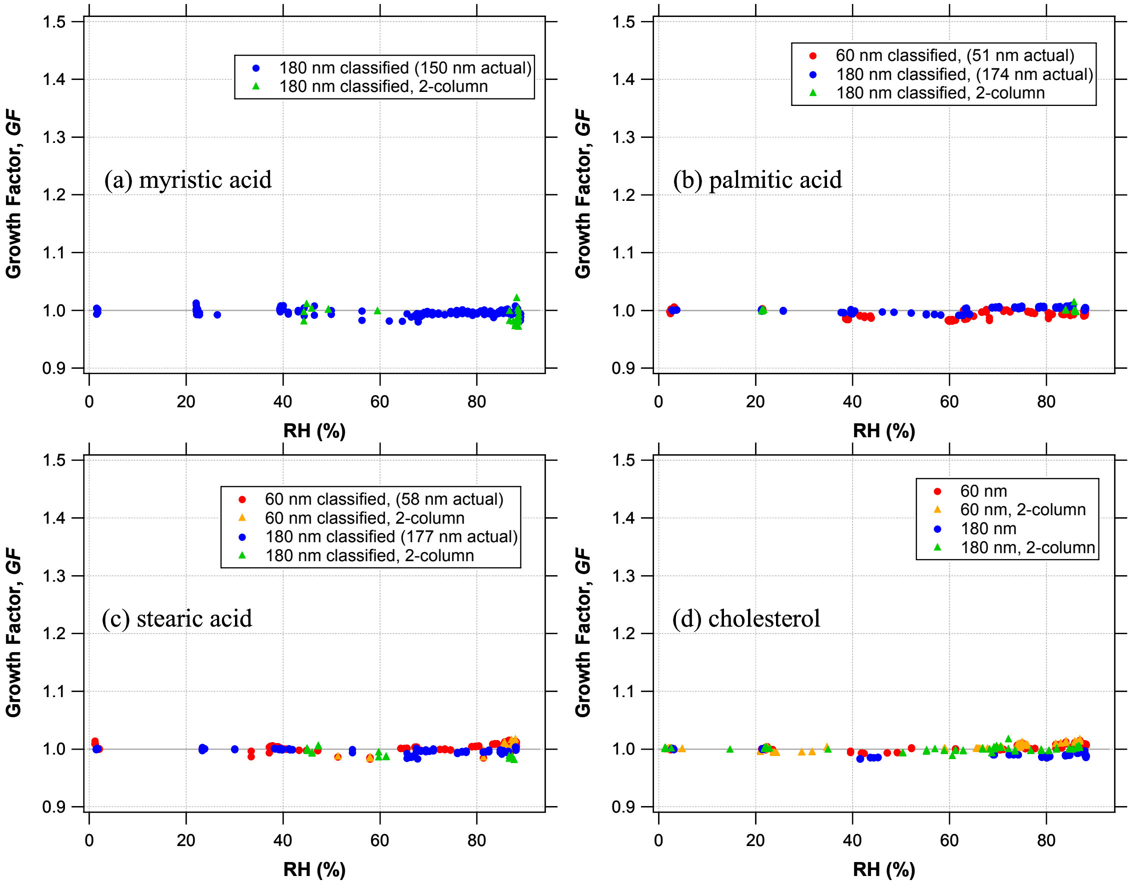

Figure 4.14. Hygroscopic growth curves of (a) myristic acid, (b) palmitic acid, (c) stearic acid, and (d) cholesterol. As expected from their high molecular weights, low solubility, and large aliphatic chains, the large fatty acids and steroid do not take up any appreciable amount of water even at high humidity and even with additional growth time.

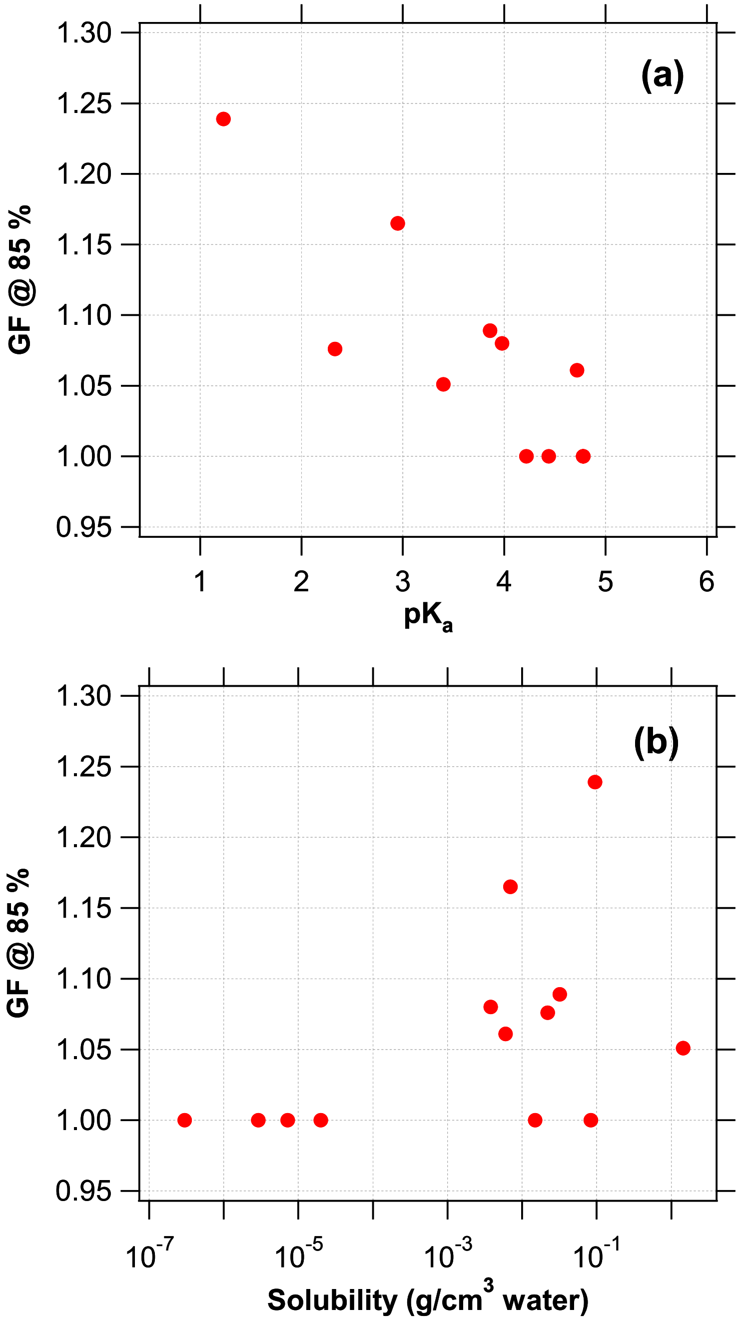

Figure 4.15. Hygroscopic growth factors at 85% RH calculated from the curve fit to the data (see Table 4.2) of various organic species plotted against (a) the pK$_a$ and (b) the water solubility of the organic compound. The data point for cholesterol is omitted from panel (a) because cholesterol does not possess an acid functional group and has a very large pK$_a$ of 15. The measured *GF*s show clear anticorrelation with the pK$_a$, which is a measure of tendency for the organic compound to keep the H+ ion from dissociating in water. The relationship between GF and water solubility is more scattered, and no clear trend is observed.